EUROPEAN ORGANISATION FOR NUCLEAR RESEARCH (CERN)

CERN-EP/2000-045
13 March 2000

Measurement of the W Mass and Width in e^+e^- Collisions at 189 GeV

The ALEPH Collaboration

Abstract

The mass of the W boson is determined in e^+e^- collisions at LEP by the direct reconstruction of W decays in $WW \to q\bar{q}q\bar{q}$ and $WW \to \ell\nu q\bar{q}$ events, supplemented by measurements using the kinematic properties of the leptons in the $WW \to \ell\nu\ell\nu$ decay channel. The main sample of W pairs is selected from an integrated luminosity of 174 pb^{-1} collected with the ALEPH detector in 1998 at a centre-of-mass energy of 188.63 GeV. The combined result from all channels is

$$m_W = 80.432 \pm 0.072(\text{stat.}) \pm 0.041(\text{syst.}) \pm 0.019(\text{FSI}) \pm 0.017(\text{LEP}) \text{ GeV}/c^2,$$

where FSI represents the possible effects of final state interactions in the $q\bar{q}q\bar{q}$ channel. In a second two-parameter fit to the $q\bar{q}q\bar{q}$, $e\nu q\bar{q}$ and $\mu\nu q\bar{q}$ channels, where the W mass and width are decoupled, the average W width is found to be $2.24 \pm 0.20(\text{stat.}) \pm 0.13(\text{syst.})$ GeV$/c^2$, consistent with the Standard Model prediction. The combination of the mass measurement presented in this paper together with those derived previously from the W pair cross section at 161 and 172 GeV and direct reconstruction at 172 and 183 GeV gives

$$m_W = 80.418 \pm 0.061(\text{stat.}) \pm 0.038(\text{syst.}) \pm 0.019(\text{FSI}) \pm 0.017(\text{LEP}) \text{ GeV}/c^2.$$

(submitted to European Physical Journal C)

The ALEPH Collaboration

R. Barate, D. Decamp, P. Ghez, C. Goy, S. Jezequel, J.-P. Lees, F. Martin, E. Merle, M.-N. Minard, B. Pietrzyk

Laboratoire de Physique des Particules (LAPP), IN^{2}P^3-CNRS, F-74019 Annecy-le-Vieux Cedex, France

R. Alemany, S. Bravo, M.P. Casado, M. Chmeissani, J.M. Crespo, E. Fernandez, M. Fernandez-Bosman, Ll. Garrido,[15] E. Graugés, M. Martinez, G. Merino, R. Miquel, Ll.M. Mir, A. Pacheco, H. Ruiz

Institut de Física d'Altes Energies, Universitat Autònoma de Barcelona, E-08193 Bellaterra (Barcelona), Spain[7]

A. Colaleo, D. Creanza, M. de Palma, G. Iaselli, G. Maggi, M. Maggi, S. Nuzzo, A. Ranieri, G. Raso, F. Ruggieri, G. Selvaggi, L. Silvestris, P. Tempesta, A. Tricomi,[3] G. Zito

Dipartimento di Fisica, INFN Sezione di Bari, I-70126 Bari, Italy

X. Huang, J. Lin, Q. Ouyang, T. Wang, Y. Xie, R. Xu, S. Xue, J. Zhang, L. Zhang, W. Zhao

Institute of High Energy Physics, Academia Sinica, Beijing, The People's Republic of China[8]

D. Abbaneo, G. Boix,[6] O. Buchmüller, M. Cattaneo, F. Cerutti, G. Dissertori, H. Drevermann, R.W. Forty, M. Frank, F. Gianotti, T.C. Greening, A.W. Halley, J.B. Hansen, J. Harvey, P. Janot, B. Jost, M. Kado, V. Lemaitre, P. Maley, P. Mato, A. Minten, A. Moutoussi, F. Ranjard, L. Rolandi, D. Schlatter, M. Schmitt,[20] O. Schneider,[2] P. Spagnolo, W. Tejessy, F. Teubert, E. Tournefier, A. Valassi, J.J. Ward, A.E. Wright

European Laboratory for Particle Physics (CERN), CH-1211 Geneva 23, Switzerland

Z. Ajaltouni, F. Badaud, G. Chazelle, O. Deschamps, S. Dessagne, A. Falvard, P. Gay, C. Guicheney, P. Henrard, J. Jousset, B. Michel, S. Monteil, J-C. Montret, D. Pallin, J.M. Pascolo, P. Perret, F. Podlyski

Laboratoire de Physique Corpusculaire, Université Blaise Pascal, IN^{2}P^3-CNRS, Clermont-Ferrand, F-63177 Aubière, France

J.D. Hansen, J.R. Hansen, P.H. Hansen,[1] B.S. Nilsson, A. Wäänänen

Niels Bohr Institute, 2100 Copenhagen, DK-Denmark[9]

G. Daskalakis, A. Kyriakis, C. Markou, E. Simopoulou, A. Vayaki

Nuclear Research Center Demokritos (NRCD), GR-15310 Attiki, Greece

A. Blondel,[12] J.-C. Brient, F. Machefert, A. Rougé, M. Swynghedauw, R. Tanaka H. Videau

Laboratoire de Physique Nucléaire et des Hautes Energies, Ecole Polytechnique, IN^{2}P^3-CNRS, F-91128 Palaiseau Cedex, France

E. Focardi, G. Parrini, K. Zachariadou

Dipartimento di Fisica, Università di Firenze, INFN Sezione di Firenze, I-50125 Firenze, Italy

A. Antonelli, G. Bencivenni, G. Bologna,[4] F. Bossi, P. Campana, G. Capon, V. Chiarella, P. Laurelli, G. Mannocchi,[1,5] F. Murtas, G.P. Murtas, L. Passalacqua, M. Pepe-Altarelli

Laboratori Nazionali dell'INFN (LNF-INFN), I-00044 Frascati, Italy

M. Chalmers, J. Kennedy, J.G. Lynch, P. Negus, V. O'Shea, B. Raeven, D. Smith, P. Teixeira-Dias, A.S. Thompson

Department of Physics and Astronomy, University of Glasgow, Glasgow G12 8QQ,United Kingdom[10]

R. Cavanaugh, S. Dhamotharan, C. Geweniger,[1] P. Hanke, V. Hepp, E.E. Kluge, G. Leibenguth, A. Putzer, K. Tittel, E. Wannemacher, S. Werner,[19] M. Wunsch[19]

Kirchhoff-Institut für Physik, Universität Heidelberg, D-69120 Heidelberg, Germany[16]

R. Beuselinck, D.M. Binnie, W. Cameron, G. Davies, P.J. Dornan, M. Girone, N. Marinelli, J. Nowell, H. Przysiezniak,[1] J.K. Sedgbeer, J.C. Thompson,[14] E. Thomson,[23] R. White

Department of Physics, Imperial College, London SW7 2BZ, United Kingdom[10]

V.M. Ghete, P. Girtler, E. Kneringer, D. Kuhn, G. Rudolph

Institut für Experimentalphysik, Universität Innsbruck, A-6020 Innsbruck, Austria[18]

C.K. Bowdery, P.G. Buck, D.P. Clarke, G. Ellis, A.J. Finch, F. Foster, G. Hughes, R.W.L. Jones, N.A. Robertson, M. Smizanska

Department of Physics, University of Lancaster, Lancaster LA1 4YB, United Kingdom[10]

I. Giehl, F. Hölldorfer, K. Jakobs, K. Kleinknecht, M. Kröcker, A.-S. Müller, H.-A. Nürnberger, G. Quast,[1] B. Renk, E. Rohne, H.-G. Sander, S. Schmeling, H. Wachsmuth, C. Zeitnitz, T. Ziegler

Institut für Physik, Universität Mainz, D-55099 Mainz, Germany[16]

A. Bonissent, J. Carr, P. Coyle, C. Curtil, A. Ealet, D. Fouchez, O. Leroy, T. Kachelhoffer, P. Payre, D. Rousseau, A. Tilquin

Centre de Physique des Particules de Marseille, Univ Méditerranée, IN^{2}P^3-CNRS, F-13288 Marseille, France

M. Aleppo, M. Antonelli, S. Gilardoni, F. Ragusa

Dipartimento di Fisica, Università di Milano e INFN Sezione di Milano, I-20133 Milano, Italy.

H. Dietl, G. Ganis, K. Hüttmann, G. Lütjens, C. Mannert, W. Männer, H.-G. Moser, S. Schael, R. Settles,[1] H. Stenzel, W. Wiedenmann, G. Wolf

Max-Planck-Institut für Physik, Werner-Heisenberg-Institut, D-80805 München, Germany[16]

P. Azzurri, J. Boucrot,[1] O. Callot, M. Davier, L. Duflot, J.-F. Grivaz, Ph. Heusse, A. Jacholkowska,[1] L. Serin, J.-J. Veillet, I. Videau,[1] J.-B. de Vivie de Régie, D. Zerwas

Laboratoire de l'Accélérateur Linéaire, Université de Paris-Sud, IN^{2}P^3-CNRS, F-91898 Orsay Cedex, France

G. Bagliesi, T. Boccali, G. Calderini, V. Ciulli, L. Foà, A. Giassi, F. Ligabue, A. Messineo, F. Palla,[1] G. Rizzo, G. Sanguinetti, A. Sciabà, G. Sguazzoni, R. Tenchini,[1] A. Venturi, P.G. Verdini

Dipartimento di Fisica dell'Università, INFN Sezione di Pisa, e Scuola Normale Superiore, I-56010 Pisa, Italy

G.A. Blair, J. Coles, G. Cowan, M.G. Green, D.E. Hutchcroft, L.T. Jones, T. Medcalf, J.A. Strong

Department of Physics, Royal Holloway & Bedford New College, University of London, Surrey TW20 OEX, United Kingdom[10]

R.W. Clifft, T.R. Edgecock, P.R. Norton, I.R. Tomalin

Particle Physics Dept., Rutherford Appleton Laboratory, Chilton, Didcot, Oxon OX11 OQX, United Kingdom[10]

B. Bloch-Devaux, P. Colas, D. Boumediene, B. Fabbro, G. Faïf, E. Lançon, M.-C. Lemaire, E. Locci, P. Perez, J. Rander, J.-F. Renardy, A. Rosowsky, P. Seager,[13] A. Trabelsi,[21] B. Tuchming, B. Vallage

CEA, DAPNIA/Service de Physique des Particules, CE-Saclay, F-91191 Gif-sur-Yvette Cedex, France[17]

S.N. Black, J.H. Dann, C. Loomis, H.Y. Kim, N. Konstantinidis, A.M. Litke, M.A. McNeil, G. Taylor

Institute for Particle Physics, University of California at Santa Cruz, Santa Cruz, CA 95064, USA[22]

C.N. Booth, S. Cartwright, F. Combley, P.N. Hodgson, M. Lehto, L.F. Thompson

Department of Physics, University of Sheffield, Sheffield S3 7RH, United Kingdom[10]

K. Affholderbach, A. Böhrer, S. Brandt, C. Grupen, J. Hess, A. Misiejuk, G. Prange, U. Sieler

Fachbereich Physik, Universität Siegen, D-57068 Siegen, Germany[16]

C. Borean, G. Giannini, B. Gobbo

Dipartimento di Fisica, Università di Trieste e INFN Sezione di Trieste, I-34127 Trieste, Italy

H. He, J. Putz, J. Rothberg, S. Wasserbaech

Experimental Elementary Particle Physics, University of Washington, WA 98195 Seattle, U.S.A.

S.R. Armstrong, K. Cranmer, P. Elmer, D.P.S. Ferguson, Y. Gao, S. González, O.J. Hayes, H. Hu, S. Jin, J. Kile, P.A. McNamara III, J. Nielsen, W. Orejudos, Y.B. Pan, Y. Saadi, I.J. Scott, J. Walsh, J.H. von Wimmersperg-Toeller, J. Wu, Sau Lan Wu, X. Wu, G. Zobernig

Department of Physics, University of Wisconsin, Madison, WI 53706, USA[11]

[1]Also at CERN, 1211 Geneva 23, Switzerland.
[2]Now at Université de Lausanne, 1015 Lausanne, Switzerland.
[3]Also at Dipartimento di Fisica di Catania and INFN Sezione di Catania, 95129 Catania, Italy.
[4]Also Istituto di Fisica Generale, Università di Torino, 10125 Torino, Italy.
[5]Also Istituto di Cosmo-Geofisica del C.N.R., Torino, Italy.
[6]Supported by the Commission of the European Communities, contract ERBFMBICT982894.
[7]Supported by CICYT, Spain.
[8]Supported by the National Science Foundation of China.
[9]Supported by the Danish Natural Science Research Council.
[10]Supported by the UK Particle Physics and Astronomy Research Council.
[11]Supported by the US Department of Energy, grant DE-FG0295-ER40896.
[12]Now at Departement de Physique Corpusculaire, Université de Genève, 1211 Genève 4, Switzerland.
[13]Supported by the Commission of the European Communities, contract ERBFMBICT982874.
[14]Also at Rutherford Appleton Laboratory, Chilton, Didcot, UK.
[15]Permanent address: Universitat de Barcelona, 08208 Barcelona, Spain.
[16]Supported by the Bundesministerium für Bildung, Wissenschaft, Forschung und Technologie, Germany.
[17]Supported by the Direction des Sciences de la Matière, C.E.A.
[18]Supported by the Austrian Ministry for Science and Transport.
[19]Now at SAP AG, 69185 Walldorf, Germany
[20]Now at Harvard University, Cambridge, MA 02138, U.S.A.
[21]Now at Département de Physique, Faculté des Sciences de Tunis, 1060 Le Belvédère, Tunisia.
[22]Supported by the US Department of Energy, grant DE-FG03-92ER40689.
[23]Now at Department of Physics, Ohio State University, Columbus, OH 43210-1106, U.S.A.

1 Introduction

The W mass has been measured at LEP from the direct reconstruction of the invariant mass of its decay products in both the WW $\rightarrow$ $q\bar{q}q\bar{q}$ hadronic and WW $\rightarrow$ $\ell\nu q\bar{q}$ semileptonic channels at centre-of-mass (CM) energies of 172 GeV in 1996 [1, 2] and 183 GeV in 1997 [3, 4]. Measurements have also been made at the Tevatron $p\bar{p}$ collider using large samples of single W's decaying into electrons and muons [5].

This paper describes a new measurement of the W mass m_W obtained by direct reconstruction from a much larger sample of data ($\sim$2.5 times) collected in 1998 with an integrated luminosity of 174.2 pb^{-1} at 188.63 GeV(subsequently indicated as 189 GeV). Supplementary information is also obtained for the first time from the WW $\rightarrow$ $\ell\nu\ell\nu$ fully leptonic channel, based on the sensitivity of the charged lepton momentum distributions and the total missing energy per event to m_W. Earlier unpublished data in this channel collected at 183 GeV with an integrated luminosity of 57.01 pb^{-1} is included and combined with the 189 GeV result. The ALEPH measurement of the W width from the fits to the reconstructed invariant mass spectra of $q\bar{q}q\bar{q}$ (4q), $e\nu q\bar{q}$ and $\mu\nu q\bar{q}$ events is also presented for the first time, using the events collected at 189 GeV.

Since the statistical error on m_W is now comparable with the previously published systematic uncertainties, a more precise evaluation of all these errors is performed. The selection of semileptonic events is refined for the higher energy, while in the 4q channel a new neural network and a new pairing algorithm are introduced, as well as an improved treatment of events in which initial state photons are identified. For the $e\nu q\bar{q}$ and $\mu\nu q\bar{q}$ channels, the former one-dimensional (1-D) Monte Carlo (MC) reweighting procedure is extended to a three-dimensional (3-D) fit, reducing the statistical error by 14% without increasing the systematic error. A new two-dimensional (2-D) reweighting fit is applied to kinematically well-fitted $\tau\nu q\bar{q}$ events, gaining a similar improvement in precision. In the 4q channel, the previous procedures developed for the mass extraction at 183 GeV [3] are retained.

The paper is organised as follows. In Sect. 2, the important properties of the ALEPH detector for this analysis are recalled. Section 3 contains a brief description of the MC event generation for the processes involved. Section 4 describes the event selection and kinematic reconstruction procedures in the different channels, highlighting, where appropriate, the modifications and improvements applied since the earlier analyses at 183 GeV [3]. Section 5 describes new features in the extraction of m_W and the evaluation of the width Γ_W. Section 6 describes all studies of systematic errors. The measurements of the W mass and width in each channel are combined in Sect. 7, taking into account common sources of systematic errors. The W masses obtained from the purely hadronic 4q channel and from the combined semileptonic and fully leptonic channels are compared in Sect. 8, together with previous results based on the data collected at 172 [1] and 183 GeV [3]. Final conclusions and their interpretation are discussed in Sect. 9.

2 The ALEPH detector

A detailed description of the ALEPH detector can be found in Ref. [6] and of its performance in Ref. [7]. Charged particles are detected in the inner part of the detector. From the beam crossing point outwards, a silicon vertex detector, a cylindrical drift

chamber and a large time projection chamber (TPC) measure up to 31 coordinates along the charged particle trajectories. A 1.5 T axial magnetic field, provided by a superconducting solenoidal coil, yields a resolution of $\delta p_T/p_T = 6 \times 10^{-4} p_T \oplus 0.005$ (p_T in GeV/c). Charged particle tracks reconstructed with at least four hits in the TPC and originating from within a cylinder of 2 cm radius and 20 cm length, centred on the nominal interaction point and parallel to the beam axis, are called *good tracks*.

Electrons and photons are identified in the electromagnetic calorimeter (ECAL) by their characteristic longitudinal and transverse shower development. The calorimeter, a lead/wire-plane sampling device with fine readout segmentation and total thickness of 22 radiation lengths at normal incidence, provides a relative energy resolution of $0.180/\sqrt{E} + 0.009$ (E in GeV). Muons are identified by their penetration pattern in the hadron calorimeter (HCAL), a 1.2 m thick iron yoke instrumented with 23 layers of streamer tubes, together with two surrounding layers of muon chambers. The hadron calorimeter also provides a measurement of the energies of charged and neutral hadrons with a relative resolution of $0.85/\sqrt{E}$ (E in GeV).

The total visible energy and momentum, and thus the missing energy, are evaluated by an energy flow reconstruction algorithm [7] which combines all of the above measurements, supplemented at low polar angles by the energy detected in the luminosity calorimeters (LCAL and SiCAL [7]) covering polar angles with respect to the beam axis down to 34 mrad. The algorithm also provides a list of charged and neutral reconstructed particles, called *energy flow objects*, from which jets are reconstructed. The four-momentum of a jet is defined as the sum of the four-momenta of all particles in the jet. The typical jet angular resolution is 30 mrad in space. The jet energy resolution is approximately $\sigma_{E_{\rm jet}} = (0.6\sqrt{E_{\rm jet}} + 0.6)$ GeV $\times (1 + \cos^2\theta_{\rm jet})$, where $E_{\rm jet}$ (in GeV) and $\theta_{\rm jet}$ are the jet energy and polar angle relative to the z axis along the e^- beam direction. A high statistics run at 91.2 GeV of 2.5 pb^{-1} at the start and 0.7 pb^{-1} near the end of running provided a large sample of Z decays for calibration.

3 Monte Carlo samples

The `KORALW` event generator, version 1.21 [8], is used to produce W pair events. Within `KORALW` all four-fermion (4-f) diagrams producing WW-like final states are computed with the `GRACE` package [9], using the fixed-width scheme for W and Z propagators. The `JETSET 7.4` [10] package with parameters tuned at the Z is used for the hadronisation of quarks in the final states. Colour reconnection and Bose-Einstein final state interactions are not included. A sample of 10^6 4-f events to all decay modes, equivalent to an integrated luminosity of 61.4 fb^{-1}, was generated with `KORALW` at a CM energy of 188.6 GeV. The W mass was set to 80.35 GeV/c^2 and the width taken from Standard Model (SM) predictions to be 2.094 GeV/c^2. This sample is used as reference sample for fitting to the data in the reweighting procedure, as well as for the study of detector systematic errors. Additional samples of ∼50k events to all decay modes were generated with W masses of up to 1.0 GeV/c^2 mass difference and separately up to 0.6 GeV/c^2 width difference from the reference sample, for checking the stability of the results. For the $\ell\nu\ell\nu$ channel, higher statistics samples of 20k fully leptonic events were generated with W masses of up to 5.0 GeV/c^2 mass difference from the reference. Also, an independent sample of 150k W pair events was generated with `KORALW` restricted to the doubly resonant CC03 diagrams [11].

This sample is used to train the neural networks and parametrise the corrections used in the kinematic fitting.

For studies of the systematic errors from fragmentation in W decays, 600k W pair events generated with KORALW were hadronised using both JETSET and HERWIG 5.9 [12], and then processed through the full detector simulation, to suppress statistical fluctuations in the comparison between the two hadronisation models. Similarly, fully simulated samples of 100k events, generated with KORALW, were hadronised with modified versions of JETSET, HERWIG and ARIADNE [13] containing various implementations of colour reconnection, to assess the influence of final state interactions between W decay products on the mass and width. Samples of KORALW events were also rehadronised with a version of JETSET that includes Bose Einstein correlations, to determine their influence on the W mass and width measurements.

Fully simulated samples of events of at least twenty times the data luminosity were generated for all background processes at 188.6 GeV. The $e^+e^- \to q\bar{q}(\gamma)$ events were generated with PYTHIA 5.7 [10] and with KORALZ [14], each with samples of ∼600k events, corresponding to an integrated luminosity of 6.0 fb^{-1}. Also, 100k ZZ, 15k Weν and 2×10^6 Zee events were generated with PYTHIA, the last with a minimum $Z^*(\gamma^*)$ invariant mass of 2 GeV/c^2. A sample of 10k Z$\nu\nu$ events produced via the W pair fusion process was also simulated using a private generator ZNNB [15]. Events with a flavour content that could originate from WW production are explicitly rejected from the ZZ and Z$\nu\nu$ samples to avoid double counting with the KORALW 4-f sample. Similarly, the Zee and Weν events are only considered if one electron escapes along the beam pipe, outside the angular cuts imposed on KORALW at generator level. Two-photon ($\gamma\gamma$) reactions into leptons and hadrons were simulated with the PHOT02 [16] and PYTHIA generators but no events survived the selection cuts in the 4q and $\ell\nu q\bar{q}$ channels. Dilepton final states were simulated using KORALZ for $\tau\tau(\gamma)$ and $\mu\mu(\gamma)$ and UNIBAB [17] for ee(γ) events.

4 Event selections and kinematic reconstruction

In the following subsections, the event selections and kinematic reconstruction procedures for the mass extraction are described for the following five classes of WW events: 4q, e$\nu q\bar{q}$, $\mu\nu q\bar{q}$, $\tau\nu q\bar{q}$ and $\ell\nu\ell\nu$. Table 1 summarises all cuts applied in the first four of these five categories. Table 2 gives the expected observable cross sections from all contributing processes for each category after all cuts, including quality criteria on the outcome of kinematic fitting, where appropriate, and the window cuts on the variables used in the mass fit. The cross sections for the WW events are calculated using the 4-f reference sample assuming $m_W = 80.35$ GeV/c^2. The number of signal events expected after all cuts from the corresponding CC03 sample is within 0.8% of the 4-f Monte Carlo prediction for all channels.

As shown in Table 2, the final number of events used in the mass analyses is on average $7 \pm 2\%$ below expectation, the hadronic channel showing the largest discrepancy. More recent theoretical calculations predict cross sections ∼2–3% below the version of KORALW used in this paper, which can explain in part this difference (see [18] and references therein).

Table 1: Summary of selection cuts used in the extraction of m_{W} by direct reconstruction of $\ell\nu\mathrm{q}\bar{\mathrm{q}}$ and 4q events (energy = [GeV], mass = [GeV/c^2], momentum = [GeV/c], angle = [degrees]).

Process	4q	eνq$\bar{\mathrm{q}}$, $\mu\nu$q$\bar{\mathrm{q}}$	$\tau\nu$q$\bar{\mathrm{q}}$
Preselection • Tracks ($\lvert\cos\theta_{\mathrm{trk}}\rvert < 0.95$) • Other cuts	$N_{\mathrm{trk}} \geq 8$ $\Sigma E_{\mathrm{trk}} \geq 0.1\sqrt{s}$ $\lvert p_L\rvert \leq 1.5(M_{\mathrm{vis}} - M_{\mathrm{Z}})$	$N_{\mathrm{trk}} \geq 5$ $\Sigma E_{\mathrm{trk}} \geq 0.1\sqrt{s}$ cuts on p_L^{miss}, E^{miss} and p_T^{miss}	$N_{\mathrm{trk}} \geq 7$ $E_{12} < 0.025\sqrt{s}$ $\cos\theta^{\mathrm{miss}} < 0.95$ hemisphere acoll. < 170 $E^{\mathrm{wedge}}_{(\vec{p}\,^{\mathrm{miss}})} < 0.20\sqrt{s}$
Semileptonic sel.		Lepton candidate: $\max(p_\ell \times \sin\alpha_{(\ell,\mathrm{jet})}/2)$ ℓ-ID in ECAL, HCAL $E_{\mathrm{e}} \to E_{\mathrm{e}} + E_{\mathrm{brems}}$ $\vec{p}_\ell \to \vec{p}_\ell + \vec{p}_{\mathrm{FSR}}$ $p_\ell \geq 22$ Electrons only: $N_{\mathrm{trk}} \geq 9$ or $p_T^{\mathrm{miss}} > 20$	Global selection: hemisphere acopl. < 175 $E^{\mathrm{wedge}}_{(\vec{p}\,^{\mathrm{miss}})} < 0.17\sqrt{s}$ $E^{\mathrm{cone}}_{(\vec{p}\,^{\mathrm{miss}})} < 0.025\sqrt{s}$ $(p^{\mathrm{miss}} + E^{\mathrm{miss}}/c)/2 < 68$ $M^{\mathrm{miss}} < 85$ $80 < M_{\mathrm{vis}} < 140$ or Topological sel.: τ + hadron jets with: di-jet acoll. > 110 $M_{\text{di-jet}} > 60$ $\max E_{\mathrm{jet}} < 70$
Jets	Force 4 hadronic jets with `DURHAM`, $y_{34} \geq 0.001$ $(E_{\mathrm{ECAL}}/E_{\mathrm{jet}})_{1^\circ} < 0.95$ $(E_{\mathrm{trk}}/E_{\mathrm{jet}}) < 0.90$	Force 2 hadronic jets with `DURHAM`	τ jet ID @ y_{cut}=0.001 with `JADE` Force 2 hadr. jets with `DURHAM`, $M_{\text{di-jet}} < 100$
NN/Probability cut	$NN > 0.3$ (14 variables)	$P > 0.4$ (E_ℓ, p_T^{miss}, isolation)	
Detected ISR	Redo 4 jets without γ, modify kinematic fit if: $(1.9 < \theta_\gamma < 11, E_\gamma > 3$ and $\lvert\theta_\gamma - \theta_{\mathrm{obj}}\rvert > 8)$ or $(\theta_\gamma > 12, E_\gamma > 5$ and $\lvert\theta_\gamma - \theta_{\mathrm{obj}}\rvert > 18)$		Reject event (in the preselection) if: $E_{\mathrm{neutral}} > 10$, isolated in 30° cone
Kinematic fitting • $P(\chi^2_{\mathrm{2C}})$ cut • masses	4C none M_1^{resc}, M_2^{resc}	1C, 2C >0.01 $M^{\mathrm{q\bar{q}}}_{\mathrm{1C}}$, $M^{\ell\nu}_{\mathrm{1C}}$, M_{2C}	2C >0.05 M_{2C}
Jet Pairing	$\max\lvert\mathcal{M}\rvert^2$ unless min $\Sigma\theta_{\text{di-jet}}$ or M_i^{resc} outside window		
Window cuts	both $60 < M_i^{\mathrm{resc}} < 86$ $\geq$one $74 < M_i^{\mathrm{resc}} < 86$	$70 < M_{\mathrm{2C}} < 90$ $0 < \sigma_{M_{\mathrm{2C}}} < 5$ $60 < M^{\mathrm{q\bar{q}}}_{\mathrm{1C}} < 110$	$74 < M_{\mathrm{2C}} < 94$ $0.5 < \sigma_{M_{\mathrm{2C}}} < 4.5$

Table 2: Expected cross sections at 189 GeV for signal and background processes after all selection, quality and window cuts for the five categories of events used in the extraction of m_{W}. All WW events are regarded as signal in the calculation of the quoted purities per channel. The $\ell\nu\ell\nu$ channel cross sections are averaged values from 183 and 189 GeV, weighted by their respective integrated luminosities. The expected signal cross sections are determined using 4-f events with $m_{\mathrm{W}} = 80.35$ GeV/c^2. For comparison, the last column of the table lists the total CC03 cross sections for each channel before any cuts.

	σ_{cuts} (pb)					σ_{tot} (pb)
Process	4q	eνq$\bar{\mathrm{q}}$	$\mu\nu$q$\bar{\mathrm{q}}$	$\tau\nu$q$\bar{\mathrm{q}}$	$\ell\nu\ell\nu$	
WW $\to$ q$\bar{\mathrm{q}}$q$\bar{\mathrm{q}}$	5.880	0.000	0.000	0.003	0.000	7.584
WW $\to$ eνq$\bar{\mathrm{q}}$	0.004	1.732	0.000	0.080	0.000	2.436
WW $\to \mu\nu$q$\bar{\mathrm{q}}$	0.003	0.000	1.844	0.045	0.000	2.436
WW $\to \tau\nu$q$\bar{\mathrm{q}}$	0.017	0.014	0.017	0.858	0.000	2.434
WW $\to \ell\nu\ell\nu$	0.000	0.000	0.000	0.000	1.144	1.760
q$\bar{\mathrm{q}}(\gamma)$	0.909	0.018	0.002	0.025	-	
ZZ	0.156	0.002	0.005	0.019	0.025	
Weν	0.000	0.005	0.000	0.010	0.011	
Zee	0.000	0.008	0.000	0.004	0.027	
ee	-	0.000	0.000	0.000	0.017	
$\mu\mu$	-	-	-	-	0.006	
$\tau\tau$	0.000	0.000	0.000	0.000	0.015	
$\gamma\gamma$	0.000	0.000	0.000	0.000	0.042	
Z$\nu\nu$	-	-	-	-	0.001	
Predicted events	1214	310	326	182	297	
Observed events	1093	290	328	173	281	
Purity (%)	84.7	98.1	99.6	94.4	88.8	

4.1 WW $\to$ q$\bar{\mathrm{q}}$q$\bar{\mathrm{q}}$ events

4.1.1 Selection

A preselection is made to suppress q$\bar{\mathrm{q}}(\gamma)$ background, where events are forced into four jets in the `DURHAM-PE` scheme as described in Ref. [1] and are only accepted if $y_{34} > 0.001$. Events with a jet which has more than 90% of its energy carried by one charged particle or which has more than 95% of its electromagnetic energy concentrated in a 1° cone around any particle are removed. A new neural network [18], trained on 189 GeV Monte Carlo events to assign output values of 0 to background and 1 to signal, is used to tag the preselected events. There are 14 input variables based on global event properties, heavy quark flavour tagging, reconstructed jet properties and WW kinematics. The signal is well separated [18] from the q$\bar{\mathrm{q}}(\gamma)$ background by requiring a neural net output $\geq$0.3. Any correlations with the $\ell\nu$q$\bar{\mathrm{q}}$ selections are ignored in the data and corresponding simulations. Indeed, after all cuts, no events were selected simultaneously by the hadronic and semileptonic selections.

According to the Monte Carlo a significant fraction ($\sim$6%) of the accepted events are accompanied by an initial state radiation (ISR) photon that can be detected in the calorimeters separately from the hadronic jets. Such photons can be removed from the

jet clustering process, thus improving the invariant mass resolution for W pairs. Studies show that such photons with energies above 3 GeV can be identified in SiCAL or LCAL or above 5 GeV in ECAL with an overall efficiency of 63% and purity of 72% if an isolation criterion based on a minimum angular separation from the closest energy flow object is applied. The minimum separation is 8° in SiCAL or LCAL and 18° in ECAL. These events are treated differently in the subsequent analysis.

4.1.2 Kinematic fitting

As in previous analyses [1, 3], a four-constraint (4C) kinematic fit employing Lagrange multipliers is applied to each selected event in data and Monte Carlo; this assumes four-momentum conservation and keeps the velocities p/E of the jets fixed to their measured values. The measured jet momenta and directions are corrected during the fit to take into account the effect of particle losses in the detector. The expectation values of these corrections and their resolutions are determined using the independent CC03 Monte Carlo sample by comparing the fully simulated jets in the detector with those built from the generated particles directly. They are parametrised by Gaussian functions in bins of jet energy and $\theta_{\rm jet}$.

For all events the fit converges successfully, producing a flat χ^2 probability distribution for $P(\chi^2) > 0.05$, as shown in Fig. 1. The peak at $P(\chi^2) < 0.05$ is populated by events that do not fully satisfy the fitting hypothesis. Monte Carlo studies show that approximately half of these events have ISR energies greater than 0.5 GeV, leading to a significant positive bias in the reconstructed di-jet masses. Most of these ISR photons escape detection by remaining in the beam pipe. However, the Monte Carlo follows well the observed performance of the kinematic fit even at low values of the χ^2 probability, and no cut on the $P(\chi^2)$ distribution is applied.

For those events with an identified ISR photon in the detector, the procedure of event clustering and fitting is modified. In this case, the remaining energy flow objects are forced into four jets. The 4C fit is performed taking into account the modified constraints

$$\left[\sum_{i=1}^{4}(E_i,\vec{p}_i) = (\sqrt{s},\vec{0})\right] \;\rightarrow\; \left[\sum_{i=1}^{4}(E_i,\vec{p}_i) = (\sqrt{s}-E_\gamma,-\vec{p}_\gamma)\right].$$

Of the 1093 data events selected after all cuts, including those described in the following section, 50 are treated in this way, compared with an expectation of 48. Monte Carlo studies show that the invariant mass resolution for these events improves from 4.1 to 2.9 GeV/c^2 and the mean displacement of the masses from their true values is zero within error. The improvement in the expected error on $m_{\rm W}$ for all selected events is 2%.

4.1.3 Jet pairing

Only one of the three possible jet pairings per event is chosen, by selecting the combination with the largest value of the matrix element $|\mathcal{M}(p_{f_1},p_{\bar{f}_2},p_{f_3},p_{\bar{f}_4},m_{\rm W}^{\rm ref})|^2$, where the p_{f_j}'s denote the fitted four-momenta of the respective jets and $m_{\rm W}^{ref}$ the reference W mass, taken to be 80.35 GeV/c^2. However, if the selected combination has the smallest sum of the two di-jet opening angles, it is replaced by the combination with the second largest value of $|\mathcal{M}|^2$.

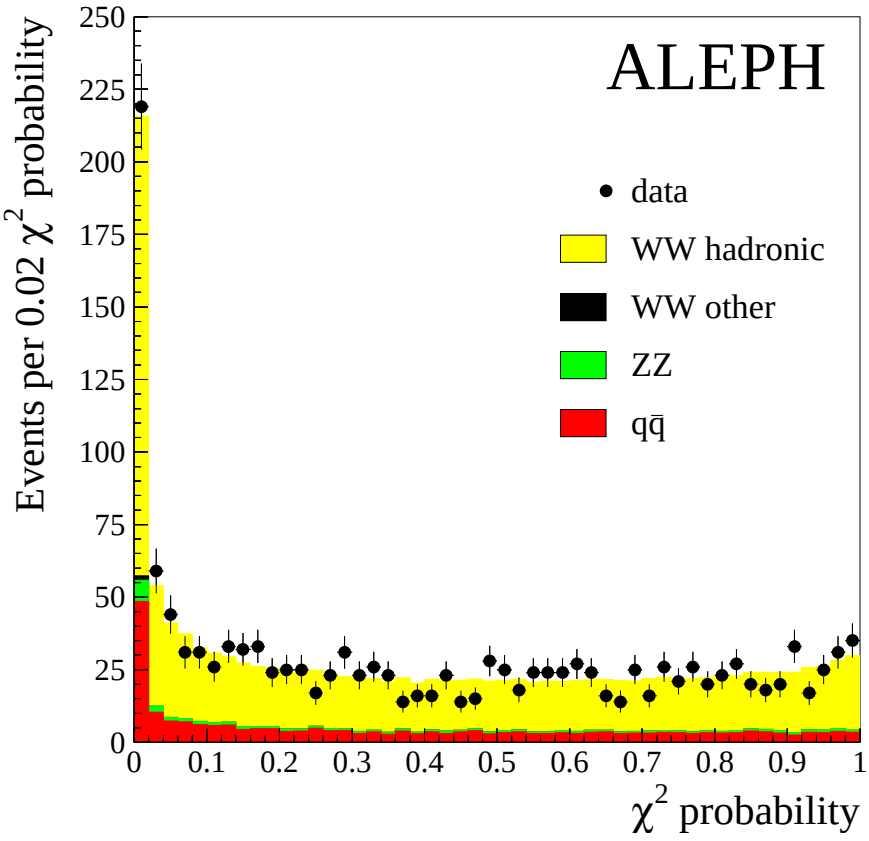

Figure 1: A comparison of the 4C kinematic fit probability distributions for data and 4q Monte Carlo events, after the neural network cut.

Two rescaled masses, each given by $m_{ij}^{\mathrm{resc}}/m_{ij} = E_{\mathrm{beam}}/(E_i + E_j)$, where E_{beam} is the beam energy and E_i, E_j are the fitted jet energies, are determined for the chosen di-jet combination. For those events with an identified ISR photon, a boost is performed to the rest frame of the four jets before mass rescaling, E_{beam} being replaced by $(\sqrt{s} - E_\gamma)/2$. Both rescaled masses for the selected combination must lie within the mass window 60 to 86 GeV/c^2 and at least one of the two masses must be between 74 and 86 GeV/c^2. If this condition is not satisfied, the combination with the second largest value of $|\mathcal{M}|^2$ is accepted instead, provided its two masses satisfy the di-jet opening angle and window criteria; otherwise the event is rejected. The combinations with the largest and second largest value of $|\mathcal{M}|^2$ are chosen in 90% and 10% of the cases, respectively. The combination with the smallest value of $|\mathcal{M}|^2$ is never considered.

The fraction of kinematically fitted signal events surviving these criteria is 80%. Of these events, 90% are found to have the correct combination of di-jets when comparing their directions to those of the original W di-quarks. The bias from the choice of reference mass is found to be negligible. The final numbers of observed and expected events are summarised in Table 2. This new algorithm selects 3% more events than the previously used algorithm based on mass difference [3], with the same probability to find the correct combination, leading to an improvement in the expected statistical error on m_{W}. In

addition, the combinatorial and physical backgrounds are flat over a wider mass range, reducing the background contamination systematic uncertainty on m_{W}.

4.2 $\mathrm{WW} \to \mathrm{e}\nu\mathrm{q}\bar{\mathrm{q}}$ and $\mathrm{WW} \to \mu\nu\mathrm{q}\bar{\mathrm{q}}$ events

4.2.1 Selection

The electron and muon semileptonic selections consider only events containing at least 5 good charged tracks. Further preselection cuts [1], based on the missing longitudinal momentum and the total visible energy, are used to suppress radiative returns to the Z and purely hadronic final states.

The lepton selection is changed with respect to previous analyses to take into account the W boost at higher CM energies. The track with the largest value of $p \times \sin(\alpha/2)$ is chosen as the lepton candidate, where p is the momentum of the track, and α is the angle between the track and the nearest jet clustered from the remaining good tracks in the event using the `DURHAM-P` algorithm with $y_{\mathrm{cut}} = 0.0003$. Loose electron and muon identification criteria are then applied.

Following closely the analysis of the 183 GeV data [3], identified electron candidates are corrected for energy losses due to bremsstrahlung in the detector material by combining their four-momenta with those of any detected photons that are consistent with this hypothesis. Both electron and muon candidates are also corrected for detected final state radiation (FSR) photons [3]. To further reduce backgrounds, mainly from $\tau\nu\mathrm{q}\bar{\mathrm{q}}$ events, a corrected momentum of at least 22 GeV/c is required for the lepton candidate. In the electron channel, at least 9 good charged tracks or 20 GeV missing transverse momentum are also required, to eliminate background from radiative Bhabha events.

The `DURHAM-PE` algorithm is used to force the remaining energy flow objects into two jets. The probability for an event to come from the signal process is determined in a three-dimensional space spanned by the lepton momentum, the missing transverse momentum and the lepton isolation [11]. The lepton isolation depends on the angle between the lepton and both the nearest good charged track and the nearest of the two jets. Events are accepted as $\mathrm{e}\nu\mathrm{q}\bar{\mathrm{q}}$ or $\mu\nu\mathrm{q}\bar{\mathrm{q}}$ candidates if the probability is 0.4 or greater.

4.2.2 Kinematic fit and quality criteria

The constraint of energy-momentum conservation is imposed on each event by performing the same kinematic fit used at 183 GeV [3]. Fits are referred to as 2C or 1C depending on whether the extra constraint that the hadronic and leptonic masses in the event be equal is also imposed. For the 1C fit two mass estimators are derived, $M_{\mathrm{1C}}^{\mathrm{q\bar{q}}}$ and $M_{\mathrm{1C}}^{l\nu}$, while only one is obtained in the case of the 2C fit, M_{2C}. The 9 (for 2C fits) or 10 (for 1C fits) parameters that cover the entire kinematically allowed phase space are varied, translating them at every iteration into the expected values for the 11 kinematic observables measured in the event, and minimising the resulting χ^2 [3]. New parametrisations of the resolutions and average corrections on the measured jet and lepton four-momenta are made for 189 GeV. Improvements are also made to reduce to less than 1% in each channel the proportion of events that fail to converge. Since event-by-event errors are used in determining the W mass, a χ^2 probability cut, $\mathcal{P}(\chi^2) > 0.01$ (see Fig. 2(a)), is applied to suppress the non-Gaussian tails of the distributions. Further cuts are then applied in the mass extraction procedure as described in the following Sect. 5.1.2 and Table 1. An event accepted by

either the eνq$\bar{\text{q}}$ or $\mu\nu$q$\bar{\text{q}}$ final selection is not considered any further in the $\tau\nu$q$\bar{\text{q}}$ analysis, so that the semileptonic samples are independent. The final number of events remaining from each channel for the measurement of the W mass is shown in Table 2.

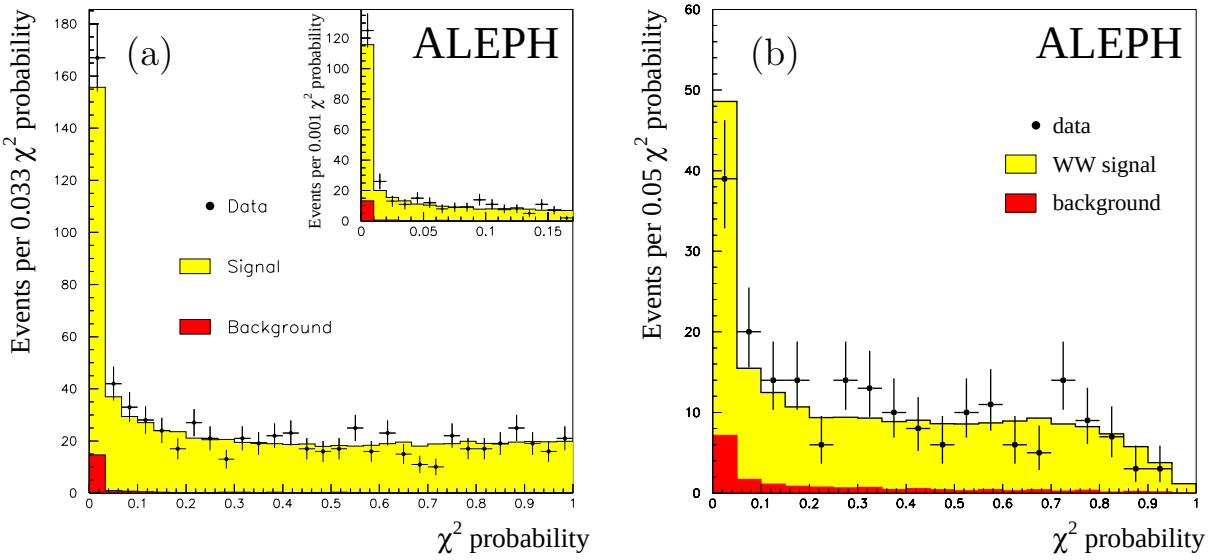

Figure 2: Comparison of the 2C kinematic fit probability distributions for data and Monte Carlo, before the $P(\chi^2)$ cut: (a) in the eνq$\bar{\text{q}}$ and $\mu\nu$q$\bar{\text{q}}$ channels combined; (b) in the $\tau\nu$q$\bar{\text{q}}$ channel.

4.3 WW $\rightarrow \tau\nu$q$\bar{\text{q}}$ events

4.3.1 Selection

The event selection is based on two complementary approaches which were developed for the measurement of the WW $\rightarrow \tau\nu$q$\bar{\text{q}}$ cross section at 161 [11] and 172 GeV [19] but are now modified to accommodate the increased boost of the W. Following a preselection, an event is accepted if it passes either a topological selection using jets or a selection based on global event properties.

The preselection requires at least seven good tracks, the energy E_{12} in a cone of 12° around the beam axis to be less than $0.025\sqrt{s}$, that there be no energetic isolated photon, and the polar angle of the missing momentum to be greater than 18.2°. The event is divided into two hemispheres by a plane perpendicular to the thrust axis. The acollinearity, calculated from the directions of the total momenta of all particles in the two hemispheres, is required to be less than 170°. The energy $E^{\text{wedge}}_{(\vec{p}\,\text{miss})}$ contained in an azimuthal wedge of half-angle 30° with respect to the plane defined by the beam and the missing momentum directions is required to be less than $0.20\sqrt{s}$.

In the topological selection, jets are constructed with the JADE algorithm using a $y_{\text{cut}} = 0.001$. The τ jet is a low multiplicity jet containing at least one and at most three tracks, with a charged momentum of at least $0.025\sqrt{s}$ and is the most antiparallel jet to the missing momentum as well as being separated by more than 20° from the other jets. The acollinearity of the hadron jets is required to be greater than 110°, their invariant mass greater than 60 GeV/c^2 with the highest jet energy being less than 70 GeV.

In the global selection, the events are required to be acoplanar and the missing momentum isolated when projected into a plane transverse to the beam axis. Thus,

the acoplanarity between the event hemispheres must be less than 175° and a tighter cut $E^{\rm wedge}_{(\vec{p}\,^{\rm miss})} < 0.17\sqrt{s}$ is applied to the energy contained in the same azimuthal wedge defined for the preselection. Also, the energy $E^{\rm cone}_{(\vec{p}\,^{\rm miss})}$ in a cone of half-angle 20° around the direction of the missing momentum is required to be less than $0.025\sqrt{s}$. In order to reduce the background from single W production, the average of the missing momentum and missing energy is required to be less than 68 GeV and the missing mass less than 85 GeV/c^2. The visible mass is required to be in the range 80–140 GeV/c^2. Unlike the cross section analyses, a τ jet and two hadronic jets are finally looked for, using the same algorithm as for the topological analysis, even for events that are accepted only by the global selection.

4.3.2 Kinematic fit and quality criteria

Since the τ jet energy is unknown due to neutrinos in the τ decay, one constraint is normally lost when fitting a $\tau\nu q\bar{q}$ event. However, the average corrections based on Monte Carlo that are made to the τ jet enable the same two-constraint fit as for the $e\nu q\bar{q}$ and $\mu\nu q\bar{q}$ events to be used. New parametrisations of these corrections and of detector resolution are determined for three separate categories of events, corresponding to the identified τ jet containing one, two or three charged tracks. The convergence rate of the kinematic fit is larger than 99% in this channel too.

Events are kept if the χ^2 probability $\mathcal{P}(\chi^2)$ from the kinematic fit is greater than 0.05 (see Fig. 2(b)), because event-by-event mass errors are used in the extraction of $m_{\rm W}$. The invariant mass of the two hadronic jets must be less than 100 GeV/c^2. Further cuts are then applied in the mass extraction procedure described in the following Sect. 5.1.3, requiring that the variables used for the reweighting fit fall within defined windows. The final number of $\tau\nu q\bar{q}$ events selected for mass extraction is summarised in Table 2.

4.4 WW $\to \ell\nu\ell\nu$ events

The selection of fully leptonic events, WW $\to \ell\nu\ell\nu$ ($\ell = e, \mu, \tau$), is the same as that used for the ALEPH cross section measurement at 183 GeV [20]. Details of the main cuts can be found in the publication of the previous analyses at 161 [11] and 172 GeV [19], of which this selection is an update. Events are accepted as WW candidates if they pass either of two selections, both of which require a low multiplicity of charged tracks, clustered together into two acoplanar energetic thin jets corresponding to the two leptons. Large missing transverse momentum is in all cases required as a signature of the two neutrinos, while a minimum invariant mass cut is used to reject leptonic gamma-gamma events, which represent the largest residual background in this channel. One analysis makes use of lepton identification to apply optimised cuts in the individual dilepton channels, while the other selection is based only on topological information. For accepted events, all the charged and neutral particles are clustered into jets using the `JADE` algorithm with a $y_{\rm cut}$ of 0.002. The energies of the two most energetic jets of each event define the variables $E_\ell^{\rm max}$and $E_\ell^{\rm min}$, which are used for the extraction of the W mass in this channel. The final numbers of observed and expected events are given in Table 2, for the 183 and 189 GeV samples combined.

5 Extraction of the W mass and width

The W boson mass and width are extracted by fitting fully simulated Monte Carlo invariant mass spectra to the observed distributions. As in previous analyses [1, 3] an unbinned maximum likelihood procedure is employed to find the best fits, using probability density functions obtained from the binned distributions of reference Monte Carlo samples, reweighting the Monte Carlo signal events with the CC03 matrix elements corresponding to various values of m_{W} and Γ_{W}. Two types of fits are performed. In the first, for all five channels individually, a one-parameter fit for m_{W} is made, where Γ_{W} varies with m_{W} according to the Standard Model as $\Gamma_{\mathrm{W}} = 2.094\ \mathrm{GeV}/c^2 \times (m_{\mathrm{W}}/(80.35\ \mathrm{GeV}/c^2))^3$. These results produce statistically the most precise value of m_{W}. In the second, for the 4q, $\mathrm{e}\nu\mathrm{q}\bar{\mathrm{q}}$ and $\mu\nu\mathrm{q}\bar{\mathrm{q}}$ channels, two-parameter fits are performed allowing m_{W} and Γ_{W} to vary as two independent parameters. Technically, the matrix element calculation assumes the Standard Model value, at a given W mass, for the coupling of electrons and their neutrinos to W bosons, while the W width is left free to vary only in the W propagator.

At LEP1, the Z mass was defined using a running-width scheme in the Breit-Wigner propagator. However, a fixed-width scheme has been employed in generating all WW events with `KORALW`. As a result, to make both mass measurements consistent with each other, a positive shift of 27 MeV/c^2 is applied to the extracted W mass [21]. The corresponding shift to the fitted width, 0.7 MeV/c^2, is also applied.

The statistical error on m_{W} and Γ_{W} is computed from the fits to the data distributions. Also, a large number of Monte Carlo subsamples are studied, each with the same number of events observed in the data, to evaluate the expected errors.

The selection efficiency is found to be independent of the W mass. However, a significant effect is found for the width, which is parametrised and included in the reweighting procedure. The variation of the total signal cross section with m_{W} affects the purity of the selected events and is taken into account, whereas its dependence on Γ_{W} is assumed to be negligible.

The reweighting procedure is tested by comparing the fitted with the input mass for each of the independent 4-f Monte Carlo samples generated with m_{W} between 79.35 and 81.35 GeV/c^2 (84.35 GeV/c^2 in the $\ell\nu\ell\nu$ channel). The same test is also performed for the measurement of the width, using input widths between 1.5 and 2.7 GeV/c^2. The relationship between the fitted and true masses (widths) is found to be linear for all channels over this range. The best straight line fits through the points are in all cases consistent with calibration curves of unit slope and zero bias, within the statistical precision of the test.

The fitted mass (width) and error are observed to be stable in all decay channels as a function of selection and mass window cuts. All results are also found to be stable and free from biases if bin sizes are varied, provided that a minimum number of reference Monte Carlo events per bin are ensured. A comparison of the shape of the data and corresponding Monte Carlo distributions is made for all variables used in the selection of events and in the choice of the best combination of di-jets in the 4q channel, observing no significant discrepancies.

5.1 W mass

5.1.1 The 4q channel

Using a binned two-dimensional (2-D) probability density function as previously [3], the likelihood fit is performed to the data distribution of the two rescaled 4C masses, within the mass windows of 60 to 86 GeV/c^2 defined by the pairing algorithm (Sect. 4.1.3). The order of the two masses in the selected combination is randomised before the fit to match the symmetrisation of the probability density function. The variable bin sizes for the Monte Carlo events are chosen both for signal and summed backgrounds so that the number of events per bin is approximately constant. A total of 324 bins are used for the signal probability density function, and 99 bins for the background.

5.1.2 The eνq$\bar{\text{q}}$ and $\mu\nu$q$\bar{\text{q}}$ channels

The one-dimensional reweighting fit [1] for the electron and muon channels is replaced by a multi-dimensional fit which allows a more complete use of the available information in each event. The following variables are used to form a three-dimensional (3-D) probability density function: the two-constraint mass $M_{2\mathrm{C}}$, the kinematic fit uncertainty $\sigma_{M_{2\mathrm{C}}}$ on the two-constraint mass and the one-constraint hadronic mass $M_{1\mathrm{C}}^{\mathrm{q\bar{q}}}$. The event-by-event correlation between $M_{1\mathrm{C}}^{\mathrm{q\bar{q}}}$ and $M_{2\mathrm{C}}$ is found to be 43%. By construction, the multi-dimensional probability density function from Monte Carlo takes into account all correlations amongst the three variables and leads to an improvement in statistical precision compared with the 1-D method of $14 \pm 1\%$. Other combinations of different variables were tested and shown to be less powerful than the above set. Using a binned 3-D probability density function, a maximum likelihood fit is performed to the data within the following acceptance windows: $70 < M_{2\mathrm{C}} < 90$ GeV/c^2, $0 < \sigma_{M_{2\mathrm{C}}} < 5$ GeV/c^2, and $60 < M_{1\mathrm{C}}^{\mathrm{q\bar{q}}} < 110$ GeV/c^2. The bin sizes for the Monte Carlo events are chosen both for signal and summed backgrounds so that the number of events per bin for each case is approximately constant. A stable mass value and statistical error are obtained when the minimum number of Monte Carlo events in any bin is 200 or greater. A conservative number of 400 events per bin is used in this analysis and leads to a three-dimensional mesh of bins of variable sizes, with 16 intervals along the $M_{2\mathrm{C}}$ axis, 3 along the $\sigma_{M_{2\mathrm{C}}}$ axis, and 10 along the $M_{1\mathrm{C}}^{\mathrm{q\bar{q}}}$ axis.

5.1.3 The $\tau\nu$q$\bar{\text{q}}$ channel

The reweighting fit for $\tau\nu\mathrm{q\bar{q}}$ candidates is similarly replaced by a 2-D reweighting fit which uses the two-constraint mass $M_{2\mathrm{C}}$ and its uncertainty $\sigma_{M_{2\mathrm{C}}}$ from the $\tau\nu\mathrm{q\bar{q}}$ kinematic fit. The events must be within the following mass and error acceptance windows: 74–94 GeV/c^2 and 0.5–4.5 GeV/c^2, respectively. The binning of the 2-D probability density function is accomplished by fixing the bin size along the event-by-event error axis to 1 GeV while varying the bin size along the 2C mass axis, for which at most 33 intervals are defined.

5.1.4 The $\ell\nu\ell\nu$ channel

The previous subsections describe the measurement of the W mass through direct reconstruction of the invariant mass of its decay products. In the WW $\to \ell\nu\ell\nu$ channel,

the kinematic properties of the leptons provide estimates of the W mass. The variables used to measure $m_{\rm W}$ are the energy of the most energetic lepton $E_\ell^{\rm max}$, the energy of the second most energetic lepton $E_\ell^{\rm min}$, and finally the missing energy $E^{\rm miss}$ of the event, defined as $\sqrt{s} - E_{\rm vis}$ where $E_{\rm vis}$ is the reconstructed visible energy of the event.

This analysis is limited by the finite Monte Carlo statistics in the tails of distributions for values of $m_{\rm W}$ far away from that used in generating the reference sample. In order to minimise this effect, a modified Monte Carlo reweighting technique was developed, in which a "running reference" probability distribution is formed from a weighted combination of independent Monte Carlo samples (at least 20k of WW $\rightarrow \ell\nu\ell\nu$ events each), generated at 10 different W masses between 79.85 GeV/c^2 and 84.35 GeV/c^2 in steps of 500 MeV/c^2. The 1-D "running reference" probability distribution for variable Y ($Y = E_\ell^{\rm max}$, $E_\ell^{\rm min}$, $E^{\rm miss}$) is constructed as the weighted sum

$$\mathcal{P}(Y, m_{\rm W}) = \frac{\sum_{i=1}^{10} w_i(m_{\rm W}) \times \mathcal{P}_i(Y, m_{\rm W}^i \rightarrow m_{\rm W})}{\sum_{i=1}^{10} w_i(m_{\rm W})},$$

where $\mathcal{P}_i(Y, m_{\rm W}^i \rightarrow m_{\rm W})$ is the probability distribution from the ith Monte Carlo sample which is generated at $m_{\rm W}^i$ and then reweighted to $m_{\rm W}$. The weight of the ith Monte Carlo sample in the running reference is given by a Gaussian function,

$$w_i(m_{\rm W}) = N_{l\nu l\nu}^i \exp\left[-\frac{(m_{\rm W}^i - m_{\rm W})^2}{\Delta^2}\right],$$

where $N_{l\nu l\nu}^i$ is the number of fully leptonic events after selection cuts in the sample. The parameter Δ is fixed to 0.7 GeV/c^2. This is small enough to reduce the weight of Monte Carlo samples which are generated far away from the fitted value of $m_{\rm W}$, thus preventing the appearance of very large weights for individual events. At the same time, this is large enough (with respect to the 500 MeV/c^2 spacing between samples) to ensure that the weight of any sample in the running reference varies slowly with $m_{\rm W}$, thus preventing a step-like behaviour for the likelihood curve.

A 1-D maximum likelihood fit is used to find the values of $m_{\rm W}$ which best fit the observed individual distributions of $E_\ell^{\rm max}$, $E_\ell^{\rm min}$ and $E^{\rm miss}$. The fit to each of the three distributions is performed by maximising the product of the likelihoods obtained from the data and reweighted Monte Carlo distributions at 183 and 189 GeV. The three different fitted $m_{\rm W}$ estimates are then combined into one estimate of $m_{\rm W}$ according to the expected correlations from Monte Carlo, which are given in Table 3. Their statistical weights in the combined average are 68.0%, 27.1% and 4.9%, respectively.

Table 3: Correlations amongst the three values of the W mass obtained from the 1-D fits to the distributions of $E_\ell^{\rm max}$, $E_\ell^{\rm min}$ and $E^{\rm miss}$ in the $\ell\nu\ell\nu$ channel.

	$m_{\rm W}(E_\ell^{\rm max})$	$m_{\rm W}(E_\ell^{\rm min})$	$m_{\rm W}(E^{\rm miss})$
$m_{\rm W}(E_\ell^{\rm max})$	1.00		
$m_{\rm W}(E_\ell^{\rm min})$	0.18 ± 0.10	1.00	
$m_{\rm W}(E^{\rm miss})$	0.45 ± 0.12	0.51 ± 0.09	1.00

5.2 W width

5.2.1 The 4q channel

In the 4q channel, the two-parameter maximum likelihood fits for m_{W} and Γ_{W} use the same 2-D probability density functions as for the mass, modified to include additional events within a wider mass window extending up to 92 GeV/c^2. Monte Carlo studies show that this window is optimal for the width, reducing the expected error by 8%, whilst having no influence on the mass. The upper bound on the rescaled 4C masses is modified accordingly in the pairing algorithm, which is otherwise the same as that for mass extraction described in Sect. 4.1.3. Except for these minor changes, event selection is also identical to that described for the measurement of the mass. The final number of observed events is 1320, compared with an expectation of 1467.

5.2.2 The eνq$\bar{\mathrm{q}}$ and $\mu\nu$q$\bar{\mathrm{q}}$ channels

For the eνq$\bar{\mathrm{q}}$ and $\mu\nu$q$\bar{\mathrm{q}}$ channels, a 1-D probability density function constructed from the M_{2C} mass estimator is used to extract Γ_{W}. The probability density function is binned in intervals of 500 MeV within a mass acceptance window of 70 to 90 GeV/c^2. Compared with the mass analysis, no cut is made on the χ^2 probability per event from the kinematic fit. Event selection is otherwise identical to that described for the measurement of the mass. The final numbers of observed events used in the fit are 330 and 360 in the $e\nu$q$\bar{\mathrm{q}}$ and $\mu\nu$q$\bar{\mathrm{q}}$ channels, compared with expectations of 352 and 366, respectively.

6 Systematic uncertainties

The following subsections describe all the systematic errors on the mass and width considered for each of the five categories of events. They are listed in Table 4 in two parts: (a) where there is some correlation between the channels and (b) where the errors are independent. Single parameter fits are used throughout in the estimation of the error on Γ_{W}, since the measured correlations between the extracted values of m_{W} and Γ_{W} are small.

6.1 Detector simulation

The reweighting procedure employed to measure the mass and width of the W relies on a correct simulation of detector effects. This requires a careful investigation of the possible discrepancies between data and the simulation, which could affect the two measurements. The main results of these studies are given in the following paragraphs.

6.1.1 Charged particle tracking

After the alignment procedure, small systematic effects remain in the momentum measurement, which are absent in the Monte Carlo simulation. These effects are proportional to momentum and opposite in sign for positively and negatively charged particles, reaching a relative difference of 2% for 45.6 GeV/c tracks at the smallest polar angles. Corrections for these distortions, determined by equalising the momenta of the two charged tracks in $\mathrm{Z} \to \mu^+\mu^-$ events, are applied to all data events. Using a large

Monte Carlo sample of events, the systematic errors on m_{W} and Γ_{W} are determined in each channel from the difference between the fitted values obtained when no correction is applied and when 50% of the correction is applied to all tracks as an estimate of the systematic uncertainty in their momenta.

6.1.2 Electron and muon systematic errors

Specific studies have been performed for electrons and muons, in addition to the tracking distortion treatment mentioned in Sect. 6.1.1.

The momentum resolution has been studied as a function of θ using $\mathrm{Z} \to \mu^+\mu^-$ decays collected during the Z calibration runs. The momentum resolution is found to be worse in data, the discrepancy with the Monte Carlo reaching a maximum of about 20% at low angle. For the measurement of the W mass and width, the electron and muon momenta in the Monte Carlo are smeared accordingly and the shifts are taken as an evaluation of the systematic errors.

Possible biases in the measurement of the lepton direction in semileptonic WW decays have been studied, as a function of the polar angle, by comparing the track polar angles as measured by the VDET with those evaluated using the TPC. No difference greater than a fraction of a milliradian has been observed. Conservatively, a 1 mrad bias has been assumed to compute the systematic error. With the same technique the lepton angular resolution has been studied. Again, no significant bias has been seen and conservatively a 1 mrad smearing has been applied to the Monte Carlo to compute the systematic error.

6.1.3 Jet energy corrections before the kinematic fit

Jets are constructed from charged and neutral particles provided by the energy flow algorithm. The jet energy before the kinematic fit is just the sum of the energies of the individual energy flow objects. Therefore, a study of di-jet events produced at the Z enables the simulation of jets with energies of $\sim$45 GeV to be directly compared with the data. This procedure makes use of all Z calibration data collected at the start and end of the LEP run in 1998, allowing a statistical precision of about 0.3% on jet energies. Figure 3 shows the ratio of measured jet energies in data to Monte Carlo as a function of jet polar angle θ_{jet}. The biases in the barrel region do not exceed 0.5% but increase to 3.5% for $|\cos\theta_{\mathrm{jet}}| > 0.95$. The Monte Carlo reconstructed jet energies are corrected bin-by-bin for these biases as a function of $\cos\theta_{\mathrm{jet}}$ before event kinematic fits are applied. The uncertainty in the determination of these corrections is used to compute a systematic error.

6.1.4 Jet energy resolution

The same technique employed to test the correctness of the jet energy scale has been used to compare the simulation of jet energy resolution. Within a precision of $\pm 2\%$, the jet energy resolution of data and Monte Carlo are in agreement over the full range $|\cos\theta_{\mathrm{jet}}| < 0.95$. For very low jet polar angles ($|\cos\theta_{\mathrm{jet}}| > 0.95$) a discrepancy of about 10% is observed. The uncertainty in the precision of this test and the size of the very low angle discrepancy are used to evaluate the systematic error.

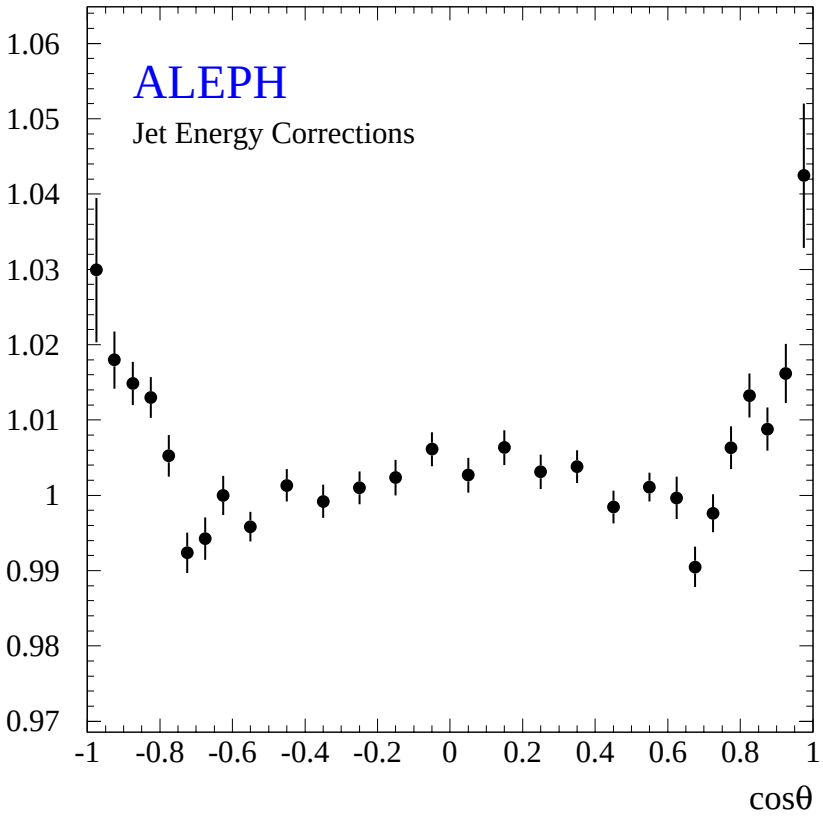

Figure 3: The ratio $\frac{(E_{\rm jet}/E_{\rm beam})_{\rm data}}{(E_{\rm jet}/E_{\rm beam})_{\rm MC}}$ derived from the comparison of jet energies at the Z peak in data taken in 1998 and Monte Carlo as a function of jet polar angle.

6.1.5 Simulation of the calorimeters

The effect of differences between data and Monte Carlo at the Z peak in the particle energy depositions, before the energy flow reconstruction, is tested by correcting the Monte Carlo at this level. The energy flow and jet energy corrections are recomputed and the measurements of $m_{\rm W}$ and $\Gamma_{\rm W}$ repeated. The differences with respect to the standard procedure described in Sect. 6.1.3 are taken as the systematic errors. This procedure is followed to check the possible effect of discrepancies in the details of the simulation, not corrected for by the average jet energy correction.

Furthermore, as the jet energy corrections are computed with data taken during the Z calibration run, any time dependent fluctuations in the calibrations of the calorimeters during the data taking at higher energy are not part of the simulation and therefore can affect the measurements. In 1998 the uncertainties in the ECAL and HCAL calibrations due to these fluctuations were at the 0.4% and 1.5% level, respectively, similar to previous years. The energy depositions in each event are therefore smeared by these amounts, independently for the two calorimeters.

Finally, the uncertainty in the energy of associated bremsstrahlung photons in $e\nu q\bar{q}$ events and of final state radiation photons in both $e\nu q\bar{q}$ and $\mu\nu q\bar{q}$ events is taken into account by varying this energy by the full uncertainty of the ECAL calibration (0.7% for

data collected in 1998). The same procedure is followed for $\ell\nu\ell\nu$ events with electrons or muons.

6.1.6 Jet angular bias

Possible discrepancies in the determination of $\theta_{\rm jet}$ are studied by comparing, both in data and in Monte Carlo, the direction of the two main jet components, charged tracks and photons. The tracking detectors and the ECAL are aligned independently but high statistics studies performed at 91.2 GeV show that their relative polar angle alignment is about 1 mrad. In order to measure angular distortions, jets belonging to data collected during the Z calibration run are selected in bins of 0.05 in $\cos\theta_{\rm jet}$ and the difference between the polar angle directions of the charged track and photon components of the same jet measured. The same procedure is repeated with the Monte Carlo showing that these differences are simulated to better than 2 mrad – the statistical precision of the test. Figure 4 shows a comparison between the Z calibration data and a fit to much higher statistics Z data collected in 1994 from an integrated luminosity of ~ 62 pb^{-1}. In the polar directions of the jet components as a function of $\cos\theta_{\rm jet}$, the mean difference is $<$1 mrad except for $\cos\theta_{\rm jet} \sim 0.8$ where simulation of the jet components in the overlap region between the barrel and endcap calorimeters is displaced from the data by up to 2 mrad. A complementary study which incorporated the third main component of the jets, the neutral hadrons, yielded similar results. The precision of these tests is taken as an upper limit for possible angular distortions and is used to compute a systematic error.

6.1.7 Jet angular resolution

Selected di-jet events from the Z calibration run have been used to measure, both in data and Monte Carlo, the jet angular resolution by comparing the angles of the two jets. The resolution is found to be slightly better in the simulation. An additional smearing of 3.5 mrad in $\theta_{\rm jet}$ and $2.6/\sin\theta_{\rm jet}$ mrad in $\phi_{\rm jet}$ has been added to the simulation to check the effect of this discrepancy on the measurements. These effects are small compared with the measured $\theta_{\rm jet}$ and $\phi_{\rm jet}$ angular resolutions of 26 mrad and $24/\sin\theta_{\rm jet}$ mrad respectively.

6.2 Fragmentation of the W $\rightarrow$ q$\bar{\rm q}$ decays

Two methods have been used to estimate the systematic uncertainty due to the fragmentation of hadronic W decays.

The first method follows that of the previous analysis [3] which is based on comparing the nominal `JETSET` fragmentation with that of `HERWIG`. The `HERWIG` fragmentation parameters used have been reoptimised at the Z taking into account flavour dependence. Specifically, the description of b into B meson fragmentation and of mean charged multiplicity $\overline{n_{\rm ch}}$ in b and udsc quark events was improved by allowing two fragmentation parameters (PSPLT and CLSMR) to vary for these two classes of events.

A large sample of 600k `KORALW` four-fermion WW events were generated, such that each event is hadronised by both models, and processed by the full detector simulation. The sample was split into subsamples and fits for $m_{\rm W}$ were performed separately for all `JETSET` and `HERWIG` subsamples. An average shift and error on the shift were determined for each channel, from the mean and spread of the difference between the two fitted masses

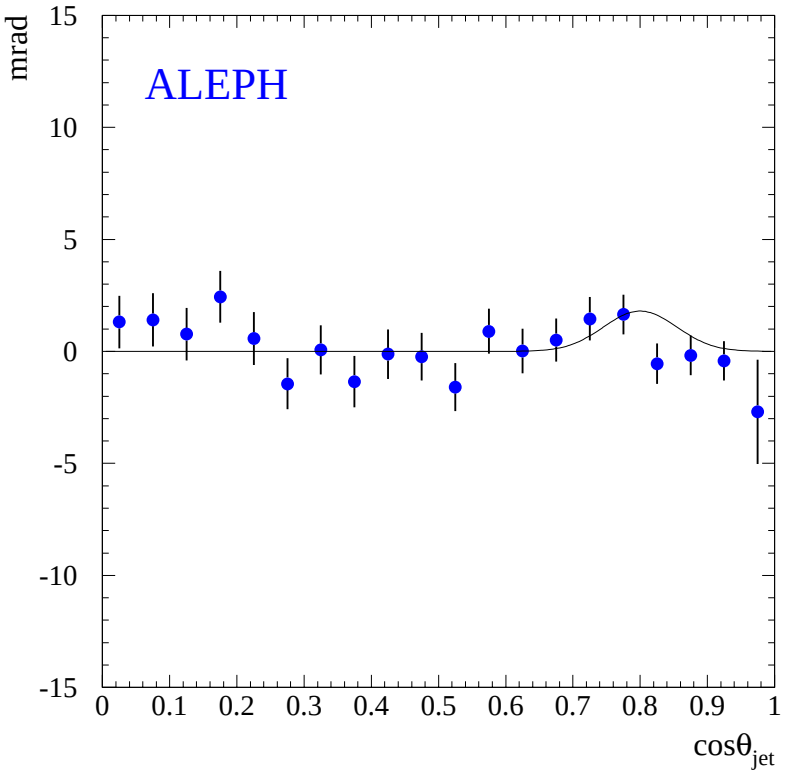

Figure 4: The mean difference, Data – MC, of $\theta_{\rm hadrons} - \theta_{\rm photons}$ as a function of $\cos\theta_{\rm jet}$ for 45 GeV jets collected in calibration runs at the Z. The continuous curve is not a fit to the plotted values, but represents a function which fits well the higher statistics Z data from 1994. $\theta_{\rm hadrons}$ and $\theta_{\rm photons}$ are the polar directions of the hadronic and photonic components of a jet.

for each subsample. The mean shift, `JETSET - HERWIG`, in $m_{\rm W}$ is determined for the 4q, eνq$\bar{\rm q}$, $\mu\nu$q$\bar{\rm q}$ and $\tau\nu$q$\bar{\rm q}$ channels to be -30 ± 10, -50 ± 20, -35 ± 20 and -11 ± 35 MeV/c^2, respectively. For $\Gamma_{\rm W}$, the shifts for the 4q, eνq$\bar{\rm q}$ and $\mu\nu$q$\bar{\rm q}$ channels are $+155\pm30$, $+65\pm30$ and $+50\pm30$ MeV/c^2, respectively.

The second method, applied only to the W mass analysis, aims to compare a Monte Carlo sample from any fragmentation model with the data, in observables that are related to the fragmentation process such as minimum jet mass. This is achieved by reweighting the distribution of such a variable so as to exactly reproduce the corresponding data distribution. These weights are then propagated through to the mass distribution to evaluate a mass shift. Many variables have been studied and the method applied twice, once with the `JETSET` sample and then with the `HERWIG` sample. Such a study shows that the new tuning of `HERWIG` is as good a description of the data as the `JETSET` Monte Carlo and that in either model the shifts per variable in $m_{\rm W}$ are not larger than 20 MeV/c^2 (hadronic channel) and 30 MeV/c^2 (semileptonic channels) relative to the data. Furthermore, the mass shifts associated with each studied variable are similar for the two fragmentation models.

The systematic errors on the W mass from the first method are quoted as they are the larger of the two methods. Also, the source of the difference between `JETSET` and `HERWIG`

in the first method has not been identified when comparing the two fragmentation models with data in the second method.

6.3 Initial state radiation

KORALW features QED initial state radiation up to $\mathcal{O}(\alpha^2 L^2)$, i.e., up to second order in the leading-log approximation. The effect of the missing higher order terms on the W mass measurement is estimated by weighting each event in a specially generated KORALW sample according to the calculated ratio of first to second order squared matrix elements: $\mathcal{O}(\alpha^1 L^1)/\mathcal{O}(\alpha^2 L^2)$. Treated as data, the weighted events selected in each channel are fitted to evaluate the mass and are compared with the corresponding unweighted events to provide an upper limit on the systematic shift.

6.4 Background contamination

For the 4q selection, the expected background remaining after all analysis cuts is 15%. The relatively small size of the data sample does not permit a detailed comparison with Monte Carlo and so the technique using Z peak data [1] to evaluate the effect of any discrepancies in the background shape and normalisation is applied again. For the latter, the effect of a 5% variation is considered.

For the semileptonic τ analysis, the effect of the uncertainties on both shape and normalisation of the background is also studied. In the e and μ channels, where the total background is a small fraction of the signal, only its normalisation is varied.

6.5 Final state interactions in the 4q channel

The possible existence of final state interactions, not reproduced by the MC simulation, between the decay products of the two W's has been suggested as a potential source of systematic uncertainties in the W mass measurement. In the 4q channel, two sources of interactions have been identified, namely colour reconnection and Bose-Einstein correlations between respectively partons and hadrons originating from different W's [21].

The effects of colour reconnection are expected to be small (below 5 MeV/c^2) during the perturbative phase [22], but could be large during the non-perturbative phase, for which only phenomenological models exist. Several of these models, which cannot be discarded by comparison with data, are used to evaluate the shifts on the W mass measurement.

The second phenomenon is simply Bose-Einstein statistics – the production of identical bosons close in momentum space is enhanced. This effect is clearly seen for pions in single Z decays at LEP1 [23] and semileptonic W decays at LEP2 [24], where the two-pion correlation function is typically studied as a function of $Q^2 = (p_1 - p_2)^2$, a measure of the distance in momentum space between pions with four-momenta p_1 and p_2. Since the W's decay so close together, the production of identical bosons from the different W's could also be enhanced, which could systematically shift the measured W boson mass.

The effect of colour reconnection and Bose-Einstein correlations has been estimated using independent MC simulations for each effect. Not having a reliable theory to predict these effects, one is forced to rely on phenomenological models and, as long as no significant effect is seen in the data itself (other than the W mass distribution), the shifts on the W

boson mass evaluated using these models are the only way to estimate possible systematic uncertainties.

6.5.1 Colour reconnection

The colour reconnection effect is studied using MC models based on variants of the parton evolution schemes in JETSET, ARIADNE and HERWIG. In all cases, the input parameters for the standard versions of these programs that do not include color reconnection are reoptimised to fit Z data.

For the JETSET study a sample of 45.6k WW $\rightarrow$ $q\bar{q}q\bar{q}$ events were generated with KORALW and then hadronised in four different ways using the standard JETSET, JETSET + model SK1 (all events are forced to be reconnected), JETSET + model SK2 and JETSET + model SK2', before being passed through the ALEPH detector simulation.

In SK2 models, strings are viewed as vortex lines with thin cores. Reconnection takes place when the core regions of two string pieces cross each other. SK2' is similar to SK2 except reconnections are only allowed if the overall string length is shortened. In these two models the probability of an event to be reconnected is fixed in the context of the model. The W mass shifts evaluated using these models are $+6 \pm 8$ MeV/c^2 for the SK2 model (29.2% of the events reconnected at 189 GeV), and $+4 \pm 8$ MeV/c^2 for the SK2' model (26.7% of the events reconnected at 189 GeV).

In the case of the SK1 model, strings are viewed as cylindrical bags with a transverse dimension of hadronic size and a Gaussian fall of the colour field density in the transverse direction. The probability $P_{\rm reco}$ for a given event to be reconnected depends on the overlap I of the colour fields as $P_{\rm reco} = 1-\exp(-k_I I)$, where k_I is a completely free parameter. For each selected value of k_I, the reconnected version of an event is kept if the corresponding value of $P_{\rm reco}$ is larger than a random number generated uniformly between 0 and 1. Otherwise, the standard non reconnected version of the event is retained to construct a mixed sample. When $k_I = 0.65$, the fraction of reconnected events is on average 29.2% in this sample, the same fraction as in the SK2 model. In this case, comparing reconnected with standard subsamples of the same originally generated events gives a mean mass shift of $+30 \pm 10$ MeV/c^2. This probabilistic procedure is different from the method used in previous publications [1, 3] where *all* events with $P_{\rm reco}$ below 30% were replaced by their standard versions (i.e., 60% of the full sample at 183 GeV).

For the ARIADNE study a sample of 45.6k WW $\rightarrow$ $q\bar{q}q\bar{q}$ events were generated with KORALW and then hadronised in three different ways using the standard ARIADNE, ARIADNE + model AR2 and ARIADNE + model AR3 and passed through the ALEPH detector simulation. In the Dipole Cascade Model [25] used in the ARIADNE event generator, the string length is determined in terms of a Λ parameter, which can be viewed as the rapidity range along the string where $\Lambda = \sum \ln(m_i^2/m_p^2)$ with m_i being the invariant mass of the string segment i and m_p setting a typical hadronic mass scale. Reconnections are allowed, within constraints of colour algebra factors, which lead to a reduction in the total Λ of the system. Model AR2 restricts reconnections to gluons with energies below $\Gamma_{\rm W}$, while model AR3 does not impose this restriction. In both models, multiple reconnections per event are permitted and reconnections may occur within the same W as well as between the two different W's. Model AR3 gives a shift $+34 \pm 34$ MeV/c^2 on the W mass. However, as gluons with energies above Γ_W are perturbative in nature and have been shown to be radiated incoherently by two initial colour dipoles [22], model AR3 is disfavoured on

theoretical grounds. It is also disfavoured by data distributions [26] and therefore is not used to assess a systematic error on the W mass. The W mass shift computed from model AR2 is $+21 \pm 19$ MeV/c^2, where 51% of all generated events are found to be reconnected at 189 GeV. For comparison, 27% of all generated events are reconnected in a simpler model ARIADNE + AR1 that allows only reconnections within the same W.

In the previous publication [3], no significant shift in m_{W} was found using HERWIG. The authors have since stated that in any case no shift should have been expected owing to a fault in the description of the space-time structure. Thus, a large sample of fully simulated events from the parton level were regenerated at 189 GeV using the corrected version with a reconnection probability of 1/9 and the parameter VMIN2, the minimum squared virtuality of partons, set to a new recommended value of 0.1 $(\mathrm{GeV}/c^2)^2$ [27]. A mean shift of $+20 \pm 10$ MeV/c^2 is found consistent with the SK1 model result.

The largest mass shift of 30 MeV/c^2, calculated using the SK1 model with a reconnection probability of 30%, is taken as the systematic error due to colour reconnection. However, there is no solid justification for choosing this probability other than its consistency with the other JETSET models.

The same samples from the JETSET and ARIADNE models were studied to find the corresponding mean shifts in Γ_{W}. Comparing the originally generated events to the colour reconnected subsamples with masses fixed to the shifted values found above yields a largest shift of $+70 \pm 20$ MeV/c^2 for the SK2' model, from which a systematic error of 70 MeV/c^2 is taken. The shift for the SK1 model with 30% reconnected events is found to be smaller, $+35 \pm 20$ MeV/c^2.

6.5.2 Bose-Einstein correlations

Only one model is considered in this study, the LUBOEI [28] implementation in JETSET. It reproduces the most visible effect of Bose-Einstein correlations – the two pion correlation function – by shifting the final state momenta of identical bosons. There are four schemes to restore energy and momentum conservation after this shuffling. All are based on the calculation of an additional shift to other pairs of particles, which need not be identical. In principle, all four schemes require tuning of parameters, including hadronisation parameters in JETSET, to match the data. Only the scheme denoted BE_3 [28] is studied here and has been tuned to LEP1 Z data [24]. Other models based on weighting techniques and studied in previous publications are not considered due to the technical difficulties to tune them to Z data at the required level of precision when large weights are involved.

A sample of 45.6k WW $\rightarrow$ $\mathrm{q\bar{q}q\bar{q}}$ events were generated with KORALW and then hadronised in three different ways: standard JETSET (no BE correlations), JETSET + LUBOEI for particles from the same W and JETSET + LUBOEI for all particles in the event, even those from different W's, before being passed through the ALEPH detector simulation.

Since the standard simulation contains no Bose-Einstein correlations at all, the systematic error of 30 MeV/c^2 in m_{W} (40 MeV/c^2 in Γ_{W}) comes from the difference between the first and the last sample, which is $+29 \pm 21$ MeV/c^2(-7 ± 40 MeV/c^2). If only particles in the same W are affected by LUBOEI, the shift in m_{W} is -3 ± 20 MeV/c^2, consistent with zero. Since recent ALEPH direct measurements [24] disfavour Bose-Einstein correlations between W's, this systematic error can be regarded as conservative.

6.6 LEP energy

The LEP beam energies are recorded every 15 minutes, or more frequently if significant shifts are observed in the RF of the accelerating cavities. The instantaneous values recorded nearest in time to the selected events are used in the analysis. Monte Carlo studies show that the relative error in the LEP energy translates into the same relative uncertainty on the fitted mass for all channels. Thus, for a LEP beam central value uncertainty of $\Delta E_{\rm beam} = 20$ MeV [29], a systematic error of $\Delta m_{\rm W} = 17$ MeV/c^2 is assigned to all the channels. For the assessment of the systematic error in $\Gamma_{\rm W}$, a Gaussian-like spread of ± 200 MeV/c^2 in the instantaneous values is also considered, but its effect is found to be smaller than that of the beam energy uncertainty; the total error amounts to ± 15 MeV/c^2.

Table 4: Summary of the correlated and uncorrelated systematic errors on $m_{\rm W}$ and $\Gamma_{\rm W}$. The larger of the shift found or its uncertainty is taken as the systematic error.

	$\Delta m_{\rm W}$ (MeV/c^2)					$\Delta\Gamma_{\rm W}$ (MeV/c^2)		
Source	4q	eνq$\bar{\rm q}$	$\mu\nu$q$\bar{\rm q}$	$\tau\nu$q$\bar{\rm q}$	$\ell\nu\ell\nu$	4q	eνq$\bar{\rm q}$	$\mu\nu$q$\bar{\rm q}$
(a) Correlated errors								
Charged tracking	<1	9	1	4	2	-	15	10
Lepton angle bias/resol$^{\rm n}$	-	15	15	-	13	-	20	20
Lepton momentum resol$^{\rm n}$	-	8	7	-	13	-	50	60
Jet energy corrections	1	4	1	5	-	5	7	6
Jet energy resolution	7	10	10	10	-	25	65	45
Calorimeter simulation	10	15	10	5	1	6	30	10
Jet angle bias/resolution	5	4	4	5	-	30	15	15
Fragmentation	30	50	35	35	-	155	65	50
Initial state radiation	2	<1	<1	<1	4	5	2	2
LEP energy	17	17	17	17	8	15	15	15
(b) Uncorrelated errors								
Reference MC Statistics	5	9	9	15	200	10	20	20
Bkgnd contamination	5	10	3	16	10	40	45	15
Colour reconnection	30	-	-	-	-	70	-	-
Bose-Einstein effects	30	-	-	-	-	40	-	-
Total (a+b)	56	61	46	47	201	185	124	99

7 The results at 189 GeV

7.1 4q channel

The mass found from the one-parameter maximum likelihood fit to the data is

$$m_{\rm W}^{\rm 4q} \;=\; 80.551 \pm 0.108({\rm stat.}) \pm 0.037({\rm syst.}) \pm 0.042({\rm FSI})\ {\rm GeV}/c^2.$$

The FSI error is taken from the Bose-Einstein and colour reconnection systematic uncertainties in quadrature. The quoted systematic error includes the LEP energy

uncertainty. The expected statistical error is ± 0.101 GeV/c^2. Figure 5(a) shows the mass distribution of the rescaled masses (two entries per event) in the window 60 to 86 GeV/c^2 compared with the Monte Carlo prediction for m_{W}=80.551 GeV/c^2.

The W total width found from the two-parameter fit to the hadronic data is

$$\Gamma_{\mathrm{W}}^{4\mathrm{q}} \;=\; 2.34 \pm 0.28(\mathrm{stat.}) \pm 0.17(\mathrm{syst.}) \pm 0.08(\mathrm{FSI})\ \mathrm{GeV}/c^2,$$

with a measured correlation of +8% between the fitted mass and width, to be compared to an expectation of $-5.5 \pm 8.1\%$. The corresponding expected statistical error is 0.25 GeV/c^2.

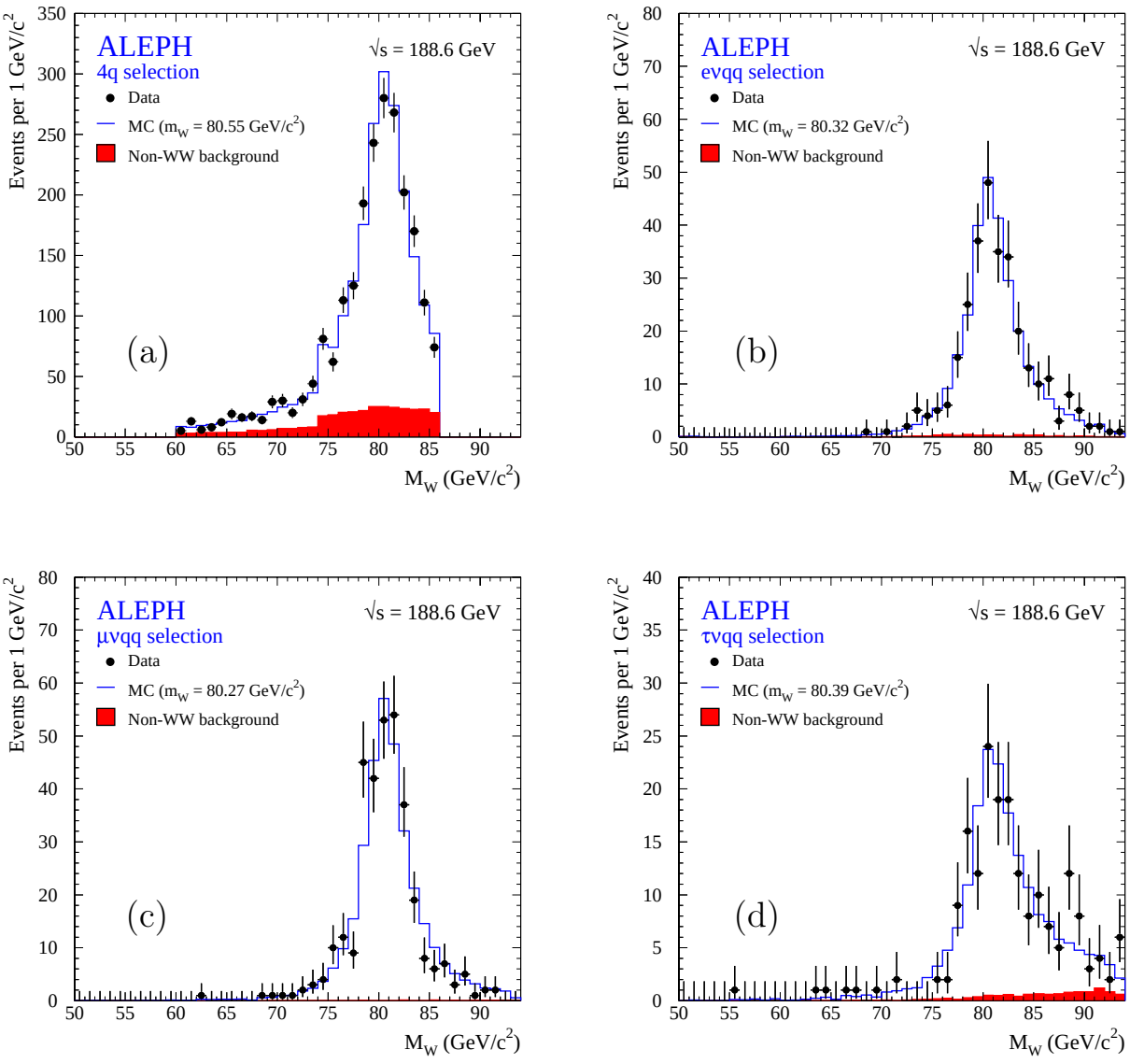

Figure 5: Mass distributions for the 4q, eνq$\bar{\mathrm{q}}$, $\mu\nu$q$\bar{\mathrm{q}}$ and $\tau\nu$q$\bar{\mathrm{q}}$ channels for data (points with error bars), non-WW background (shaded area) and signal+background Monte Carlo with m_{W} values set to those fitted from each individual channel (solid line histogram). The distribution in the 4q channel is restricted to the window defined by the pairing algorithm, $60 < M_W < 86$ GeV/c^2, as the pair of jets whose invariant mass should be plotted is uniquely defined only for these events.

7.2 eνq$\bar{\text{q}}$, $\mu\nu$q$\bar{\text{q}}$ and $\tau\nu$q$\bar{\text{q}}$ channels

The results from the one-parameter fit to the data, with the statistical and systematic errors including the LEP energy, are

$$\begin{aligned} m_{\mathrm{W}}^{\mathrm{e}\nu\mathrm{q}\bar{\mathrm{q}}} &= 80.319 \pm 0.154(\mathrm{stat.}) \pm 0.061(\mathrm{syst.})\ \mathrm{GeV}/c^2, \\ m_{\mathrm{W}}^{\mu\nu\mathrm{q}\bar{\mathrm{q}}} &= 80.272 \pm 0.141(\mathrm{stat.}) \pm 0.046(\mathrm{syst.})\ \mathrm{GeV}/c^2, \\ m_{\mathrm{W}}^{\tau\nu\mathrm{q}\bar{\mathrm{q}}} &= 80.385 \pm 0.287(\mathrm{stat.}) \pm 0.047(\mathrm{syst.})\ \mathrm{GeV}/c^2. \end{aligned}$$

The expected errors are ± 0.150, ± 0.139 and ± 0.286 GeV/c^2 for the e, μ and τ semileptonic channels, respectively. Figures 5 (b), (c) and (d) display the mass distributions resulting from the 2C kinematic fit to semileptonic final states for data. For comparison the mass distribution predicted from Monte Carlo, reweighted to the fitted W mass in data, is superimposed on each figure. The combined mass for the semileptonic channels from the one-parameter fits is

$$m_{\mathrm{W}}^{\ell\nu\mathrm{q}\bar{\mathrm{q}}} = 80.304 \pm 0.098(\mathrm{stat.}) \pm 0.050(\mathrm{syst.})\ \mathrm{GeV}/c^2,$$

with a χ^2/dof of 0.14/2.

A two-parameter fit to the data gives the following results for the W total width:

$$\begin{aligned} \Gamma_{\mathrm{W}}^{\mathrm{e}\nu\mathrm{q}\bar{\mathrm{q}}} &= 2.47 \pm 0.46(\mathrm{stat.}) \pm 0.12(\mathrm{syst.})\ \mathrm{GeV}/c^2, \\ \Gamma_{\mathrm{W}}^{\mu\nu\mathrm{q}\bar{\mathrm{q}}} &= 1.99 \pm 0.35(\mathrm{stat.}) \pm 0.10(\mathrm{syst.})\ \mathrm{GeV}/c^2, \end{aligned}$$

where the expected errors are determined to be ± 0.41 and ± 0.38 GeV/c^2 for the e and μ channels, respectively. The measured correlation from the fit to the data between m_{W} and Γ_{W} is -4.0% and -6.2% for the eνq$\bar{\text{q}}$ and $\mu\nu$q$\bar{\text{q}}$ channels, respectively. The expected values from Monte Carlo are $-16 \pm 10\%$ and $-8 \pm 10\%$, respectively.

The combined total width from the two-parameter fits in the eνq$\bar{\text{q}}$ and $\mu\nu$q$\bar{\text{q}}$ channels is

$$\Gamma_{\mathrm{W}}^{\ell\nu\mathrm{q}\bar{\mathrm{q}}} = 2.17 \pm 0.28(\mathrm{stat.}) \pm 0.10(\mathrm{syst.})\ \mathrm{GeV}/c^2,$$

with a χ^2/dof of 0.67/1.

7.3 $\ell\nu\ell\nu$ channel

The mass measured in the $\ell\nu\ell\nu$ channel from 57 pb^{-1} of data taken at $\sqrt{s} = 183$ GeV together with 174 pb^{-1} of data taken at $\sqrt{s} = 189$ GeV is

$$m_{\mathrm{W}}^{\ell\nu\ell\nu} = 81.81 \pm 0.67(\mathrm{stat.}) \pm 0.20(\mathrm{syst.})\ \mathrm{GeV}/c^2.$$

In this case, the result of the measurement is quoted with its expected error rather than with the fit error, that amounts to ± 0.48 GeV/c^2. This is because, due to the small size of the data sample, the statistical error from the fit has a large uncertainty of 0.3 GeV/c^2. Figure 6 shows the distributions of $E_\ell^{\max}$, $E_\ell^{\min}$ and E^{miss} in data, compared with those predicted from Monte Carlo reweighted to the fitted value of m_{W} from this channel alone.

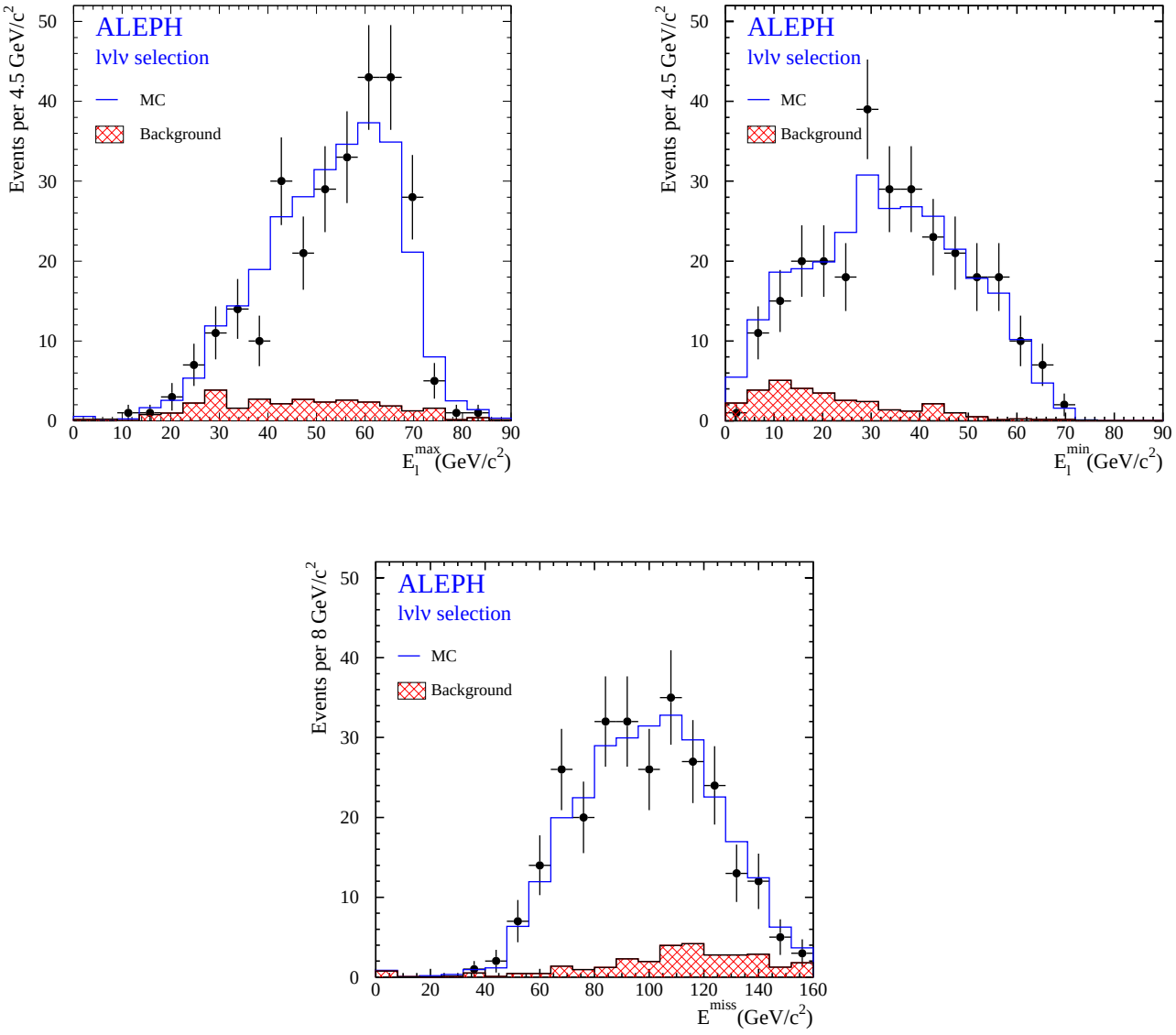

Figure 6: The distributions of the higher and lower lepton momenta and of the missing energy in each $\ell\nu\ell\nu$ event at 189 GeV, compared with the reweighted Monte Carlo prediction giving the best combined fit.

7.4 All channels

The combined mass and width from all channels are

$$\begin{aligned} m_{\mathrm{W}} &= 80.432 \pm 0.072(\mathrm{stat.}) \pm 0.044(\mathrm{syst.}) \pm 0.019(\mathrm{FSI})\ \mathrm{GeV}/c^2, \\ \Gamma_{\mathrm{W}} &= 2.24 \pm 0.20(\mathrm{stat.}) \pm 0.13(\mathrm{syst.})\ \mathrm{GeV}/c^2. \end{aligned}$$

The LEP energy uncertainty has been added in quadrature to the mass and width systematic errors. The χ^2/dof is 1.94/1 and 0.18/1 for the mass and width combinations, respectively.

8 W masses from the 4q and non-4q channels.

The mass values from the hadronic (4q) and semileptonic ($\ell\nu q\bar{q}$) analyses obtained at 189 GeV can be combined with those determined at 172 GeV and 183 GeV by the same methods. The results from the fully leptonic channel at 189 and 183 GeV are combined with the semileptonic masses found at 189 GeV to produce a "non-4q" mass at this energy, with a χ^2/dof of 4.68/3. Table 5 lists all 4q and non-4q mass values derived by ALEPH. Systematic errors in this table differ from those previously published because the present estimate of FSI errors in the hadronic channel has been propagated to the earlier measurements.

Table 5: W masses measured from purely hadronic (4q) and a combination of fully leptonic and semileptonic (non-4q) decay events. The uncertainties quoted are the statistical and systematic errors, in this order. Systematic errors include the LEP beam energy uncertainty and the FSI error.

$\sqrt{s}$ (GeV)	$m_{\mathrm{W}}^{\mathrm{4q}}$ (GeV/c^2)	$m_{\mathrm{W}}^{\text{non-4q}}$ (GeV/c^2)
172 [1]	$81.30 \pm 0.47 \pm 0.10$	$80.38 \pm 0.43 \pm 0.13$
183 [3]	$80.461 \pm 0.177 \pm 0.065$	$80.326 \pm 0.184 \pm 0.040$
189	$80.551 \pm 0.108 \pm 0.056$	$80.339 \pm 0.097 \pm 0.050$

These measurements of $m_{\mathrm{W}}^{\mathrm{4q}}$ and $m_{\mathrm{W}}^{\text{non-4q}}$ are combined by minimising a χ^2 built from the full covariance matrix taking into account all correlations between different channels and different years, including correlations in the LEP beam energy uncertainty between different years. First, all measurements are fitted to obtain the average $m_{\mathrm{W}}^{\mathrm{4q}}$ and $m_{\mathrm{W}}^{\text{non-4q}}$, considered as two different physical parameters, in order to investigate whether there is a significant difference due to final state interactions not properly described in the Monte Carlo. At this stage all systematic uncertainties are taken into account including the FSI error. The resulting averaged 4q and non-4q masses are

$$\begin{aligned} \langle m_{\mathrm{W}}^{\mathrm{4q}} \rangle &= 80.554 \pm 0.090(\text{stat.}) \pm 0.036(\text{syst.}) \pm 0.042(\text{FSI}) \pm 0.017(\text{LEP}) \text{ GeV}/c^2, \\ \langle m_{\mathrm{W}}^{\text{non-4q}} \rangle &= 80.335 \pm 0.084(\text{stat.}) \pm 0.045(\text{syst.}) \pm 0.017(\text{LEP}) \text{ GeV}/c^2. \end{aligned}$$

with a χ^2/dof of 2.76/4. A second fit is performed to extract the difference between hadronic and leptonic masses when the FSI error from Bose-Einstein correlations and colour reconnection is *not* included, yielding

$$\langle m_{\mathrm{W}}^{\mathrm{4q}} \rangle - \langle m_{\mathrm{W}}^{\text{non-4q}} \rangle = +0.219 \pm 0.124 \text{ (stat.} + \text{syst.) GeV}/c^2 \ ,$$

to be compared with the 0.042 GeV/c^2 FSI uncertainty.

9 Conclusions and interpretation

Fully hadronic W decays are selected using a neural network method, while the semileptonic decays are identified individually using three separate selections. The mass variables are determined in a four-constraint fit with rescaling for the 4q channel, and in one- and two-constraint fits for the semileptonic channels. The resulting invariant mass

distributions are compared with reweighted Monte Carlo events, and values of the W mass are extracted in maximum likelihood fits.

From all channels the average W mass from the 189 GeV data is

$$m_{\mathrm{W}} = 80.432 \pm 0.072(\mathrm{stat.}) \pm 0.041(\mathrm{syst.}) \pm 0.019(\mathrm{FSI}) \pm 0.017(\mathrm{LEP})\ \mathrm{GeV}/c^2,$$

where the theoretical error is due to Bose-Einstein and colour reconnection uncertainties and the last error is due to the LEP energy uncertainty.

The W width is also determined by a reweighting procedure from the invariant mass distributions of 4q, eνq$\bar{\mathrm{q}}$ and $\mu\nu$q$\bar{\mathrm{q}}$ events. The combined result for the three channels is

$$\Gamma_{\mathrm{W}} = 2.24 \pm 0.20(\mathrm{stat.}) \pm 0.13(\mathrm{syst.})\ \ \mathrm{GeV}/c^2.$$

Finally, a fit is performed to all measurements of the W mass at 172, 183 and 189 GeV, together with the earlier ALEPH results obtained from the total W pair cross sections at 161 [11] and 172 GeV [19]. With a χ^2/dof of 6.19/6, the combination of all ALEPH measurements of the W mass is

$$m_{\mathrm{W}} = \ \ 80.418 \pm 0.061(\mathrm{stat.}) \pm 0.038(\mathrm{syst.}) \pm 0.019(\mathrm{FSI}) \pm 0.017(\mathrm{LEP})\ \mathrm{GeV}/c^2.$$

The precision achieved for this W mass measurement is sensitive to the pure weak radiative corrections in the Standard Model. The relationship can be written (see for example Ref. [30])

$$m_{\mathrm{W}}^2 \left(1 - \frac{m_{\mathrm{W}}^2}{m_{\mathrm{Z}}^2}\right) \ = \ \frac{\pi\alpha}{G_\mu\sqrt{2}} \left(1 + \Delta r_w + \Delta\alpha\right),$$

where Δr_w results from the effects of the pure weak radiative corrections and $\Delta\alpha = 0.0632 \pm 0.0007$ [31] is the photon vacuum polarisation. Using the values for G_μ, α^{-1} and m_{Z} given in Refs. [32, 33], the above measurement of the W mass, $m_{\mathrm{W}} = 80.418 \pm 0.076$ GeV, yields

$$\Delta r_w = -0.0290 \pm 0.0049,$$

demonstrating the need for pure weak radiative corrections at the level of 5.9 standard deviations.

Acknowledgements

It is a pleasure to congratulate our colleagues from the CERN accelerator divisions for the very successful operation of LEP2. We are indebted to the engineers and technicians in all our institutions for their contributions to the excellent performance of ALEPH. Those of us from non-member countries thank CERN for its hospitality.

References

[1] ALEPH Collaboration, *Measurement of the W mass by Direct Reconstruction in* $\mathrm{e^+e^-}$ *collisions at 172* GeV, Phys. Lett. B422 (1998) 384.

[2] DELPHI Collaboration, *Measurement of the W-pair cross section and of the W mass in* e^+e^- *interactions at 172 GeV*, Eur. Phys. J. C2 (1998) 581;
L3 Collaboration, *Measurements of the Mass, Width, and Gauge Couplings of the W Boson at LEP*, Phys. Lett. B413 (1997) 176;
OPAL Collaboration, *Measurements of the W boson mass and* WW *production and decay properties in* e^+e^- *collisions at 172 GeV*, Eur. Phys. J. C1 (1998) 395.

[3] ALEPH Collaboration, *Measurement of the W mass by Direct Reconstruction in* e^+e^- *collisions at 183* GeV, Phys. Lett. B453 (1999) 121.

[4] DELPHI Collaboration, *Measurement of the mass of the W boson using direct reconstruction at* $\sqrt{s}$ *= 183 GeV*, Phys. Lett. B462 (1999) 410;
L3 Collaboration, *Measurement of the Mass and Width of the W Boson at LEP*, Phys. Lett. B454 (1999) 386;
OPAL Collaboration, *Measurement of the W mass and width in* e^+e^- *collisions at 183 GeV*, Phys. Lett. B453 (1999) 138.

[5] CDF Collaboration, *A measurement of the W boson mass*, Phys. Rev. D52 (1995) 4784;
DØ Collaboration, *Measurement of the W boson mass at the Fermilab* $p\bar{p}$ *collider*, Phys. Rev. Lett. 80 (1998) 3008.

[6] ALEPH Collaboration, *ALEPH: A detector for electron-positron annihilations at LEP*, Nucl. Inst. Meth. A 294 (1990) 121.

[7] ALEPH Collaboration, *Performance of the ALEPH detector at LEP*, Nucl. Inst. Meth. A 360 (1995) 481.

[8] M. Skrzypek, S. Jadach, W. Placzek and Z. Wąs, Comp. Phys. Commun. 94 (1996) 216.

[9] GRACE Manual, MINAMI-TATEYA group, KEK report 92-19 (1993).

[10] T. Sjöstrand, Comp. Phys. Commun. 82 (1994) 74.

[11] ALEPH Collaboration, *Measurement of the W mass in* e^+e^- *collisions at production threshold*, Phys. Lett. B401 (1997) 347.

[12] G. Marchesini et al., Comp. Phys. Commun. 67 (1992) 465.

[13] L. Lönnblad, Comp. Phys. Commun. 71 (1992) 15.

[14] S. Jadach, B.F.L. Ward, and Z. Wąs, Comp. Phys. Commun. 79 (1994) 503.

[15] The `ZNNB` generator is based on the differential cross sections published in
S. Ambrosanio and B. Mele, Nucl. Phys. B374 (1992) 3.

[16] ALEPH Collaboration, *An experimental study of* $\gamma\gamma \to$ *hadrons at LEP*, Phys. Lett. B313 (1993) 509.
J. A. M. Vermasseren in *Proceedings of the IVth International Workshop on Gamma-Gamma Interactions*, Eds. G. Cochard and P. Kessler, Springer Verlag (1980).

[17] H. Anlauf et al., Comp. Phys. Commun. 79 (1994) 466.

[18] ALEPH Collaboration, *Measurement of W-pair cross section in* e^+e^- *collisions at 189 GeV*, in preparation.

[19] ALEPH Collaboration, *Measurement of W-pair cross section in* e^+e^- *collisions at 172 GeV*, Phys. Lett. B415 (1997) 435.

[20] ALEPH Collaboration, *Measurement of W-pair cross section in* e^+e^- *collisions at 183 GeV*, Phys. Lett. B453 (1999) 107.

[21] *Determination of the mass of the* W *boson*, in *Physics at LEP2*, CERN 96-01, eds. G. Altarelli, T. Sjöstrand and F. Zwirner, vol. 1, p. 141.

[22] T. Sjöstrand and V.A. Khoze, Z. Phys. C62 (1994) 281; Phys. Rev. Lett. 72 (1994) 28.

[23] OPAL collaboration, *Transverse and longitudinal Bose-Einstein correlations in hadronic* Z^0 *decays*, OPAL PN387.

[24] ALEPH collaboration, *Bose-Einstein correlations in W-pair decays*, CERN-EP/99-173, submitted to Phys. Lett. B.

[25] G. Gustafson, Phys. Lett. B175 (1986) 453; G. Gustafson and U. Pettersson, Nucl. Phys. B306 (1988) 746.

[26] OPAL collaboration, *Colour reconnection studies in* $e^+e^- \to W^+W^-$ *at* $\sqrt{s} = 183$ *GeV*, Phys. Lett. B453 (1999) 153.

[27] B. Webber, private communication.

[28] L. Lönnblad and T. Sjöstrand, *Modelling Bose-Einstein correlations at LEP2*, Eur. Phys. J. C2 (1998) 165.

[29] LEP energy working group, *Evaluation of the LEP Centre-of-Mass energy above the* WW *production threshold*, CERN-EP/98-191, submitted to Eur. Phys. J. C.

[30] *WW cross sections and distributions*, in *Physics at LEP2*, CERN 96-01, eds. G. Altarelli, T. Sjöstrand and F. Zwirner, vol. 1, p. 79.

[31] S. Eidelman and F. Jegerlehner, Z. Phys. C67 (1995) 585;
H. Burkhardt and B. Pietrzyk, Phys. Lett. B356 (1995) 398.

[32] The Particle Data Group, C. Caso et al., Eur. Phys. J. C3 (1998) 1.

[33] The LEP collaborations ALEPH, DELPHI, L3, OPAL, the LEP Electroweak Working Group, and the SLD Heavy Flavour and Electroweak Groups, *A Combination of Preliminary Electroweak Measurements and Constraints on the Standard Model*, CERN-EP/2000-16.